Available online at www.sciencedirect.com
SCIENCE DIRECT®
Journal of Computational Physics 189 (2003) 239–276
JOURNAL OF COMPUTATIONAL PHYSICS
www.elsevier.com/locate/jcp

Coupling of the Wang Chang–Uhlenbeck equations with the multispecies Euler system

Stéphane Dellacherie *

Commissariat à l'Énergie Atomique, 91191 Gif sur Yvette, France

Received 23 September 2002; received in revised form 12 March 2003; accepted 1 April 2003

Abstract

After having recalled the basic properties of the Wang Chang–Uhlenbeck equations, we describe a class of relaxation schemes to solve the multispecies Euler system closed with a non-classical state equation, system which is the fluid limit of these kinetic equations. Then, we show how to couple the resolution of the Wang Chang–Uhlenbeck equations with the resolution of this Euler system by using a particular relaxation scheme – namely, a kinetic scheme – which allows to define a natural boundary condition at the kinetic–fluid interface and by using a Marshak condition to take into account the effect of the Knudsen layer in the fluid domain through an asymptotic matching. Finally, we show applications in the field of the Atomic Vapor Laser Isotopic Separation (AVLIS).

Keywords: Multispecies Boltzmann and Euler equations; Relaxation schemes; Kinetic schemes; Entropic schemes; Marshak condition; Domain decomposition; Knudsen layer; Isotopic separation

1. Introduction

The aim of the Atomic Vapor Laser Isotopic Separation (AVLIS; SILVA in french) is to separate uranium-235 from uranium-238 to obtain the fuel for nuclear plants (cf. [1]). Indeed, the natural uranium-235 isotopic abundance is of about 0.7% and, to obtain the fissile fuel, we need to increase this abundance to about 4%. From this point of view, the AVLIS process vaporizes uranium by using an intense electronic beam which heats an uranium liquid source up to 3000 K (the uranium output is of some kilograms per hour). Then, the uranium vapor is irradiated by a laser beam which ionizes the uranium-235 (and, ideally, not the uranium-238) further collected as a liquid on collectors which are negative electrodes, see Fig. 1. Moreover, to diminish the liquefaction temperature of the uranium on the electrodes (through the eutectic effect), iron is added in the uranium source.

* Tel.: +33-1-6908-1511.
E-mail address: stephane.dellacherie@cea.fr.

0021-9991/03/$ - see front matter
doi:10.1016/S0021-9991(03)00210-9

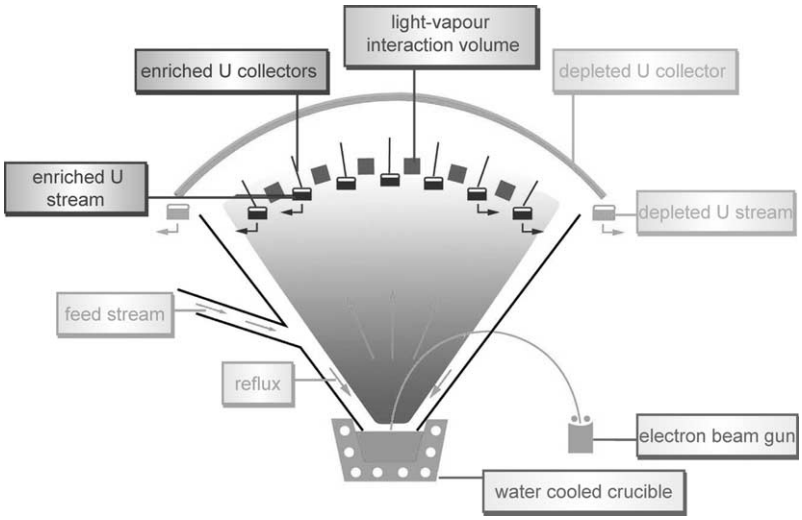

Fig. 1. Vacuum chamber of the evaporation AVLIS process.

To describe the stationary uranium–iron gas mixture expansion, we use the Wang Chang–Uhlenbeck equations (cf. [2,3]) – also named Wang Chang–Uhlenbeck-de Boer (WCUB) equations or semi-classical multispecies Boltzmann equations – for two reasons:

- *the first reason* comes from the fact that the uranium–iron gas mixture is almost rarefied, which induces that the expansion has to be described with a kinetic formalism of the Boltzmann type;
- *the second reason* is due to the fact that the high temperature of the gas mixture induces quantified energy transfers between the electronic metastable energy levels of uranium and iron atoms: that is why we have to use also a semi-classical formalism.

Some papers have already focuss on the simulation of these Wang Chang–Uhlenbeck equations for AVLIS applications, see [5–8].

An other important feature of the AVLIS expansion is that near the source of uranium–iron, it exists a tiny area where the vapor is very dense – thus, the mixture is almost at the thermodynamic equilibrium in this area – which makes the CPU time and the computer memory used to discretize the Wang Chang–Uhlenbeck equations dramatically increase. To diminish the CPU time and the required computer memory, we discretize the fluid limit of the Wang Chang–Uhlenbeck equations in the dense area where the gas mixture is at the thermodynamic equilibrium – i.e., in the fluid area – limit which is the multispecies Euler system closed with a non-classical state equation. Of course, in the remaining part of the physical domain – i.e., in the rarefied or kinetic area – we solve the Wang Chang–Uhlenbeck equations. In other words, we have to solve a domain decomposition problem which is named here *kinetic–fluid coupling*.

Moreover, between the uranium–iron source and the fluid area, the gas mixture is not at the thermodynamic equilibrium although it is very dense: this very tiny area is called *Knudsen layer*. To optimize the gain in CPU time and in computer memory, we would like to *asymptotically match* the fluid area where the Euler system is solved with the uranium–iron source.

Thus, the aim of this paper is to expose the kinetic–fluid coupling technique and the asymptotic matching technique designed for the evaporation AVLIS process.

Let us note that the techniques and results presented in this paper can be extended to other *strong* evaporation problems as for example for the description of the gas expansion in the coma of a comet produced by sun radiations (cf. [9]) or for the description of a volcanic jet when the atmosphere of the

planet is rarefied as on the Jupiter's moon Io (cf. [10]). Besides, the authors of the paper [10] propose to divide the physical domain in several subdomains and to use a particular time step in each subdomain to overcome the difficulty of having a dense area and a rarefied area in the resolution of the kinetic model.

The technique chosen to obtain a good boundary condition between the kinetic and fluid domains extends to the semi-classical multispecies case the technique already proposed in [11] for classical aerodynamics problems (see also [12] and the references herein). This technique uses a kinetic scheme (cf. [14]) in the fluid domain to discretize the Euler system: this finite volume scheme allows to define a natural boundary condition at the kinetic–fluid interface with *no overlapping* between the kinetic and the fluid domains, this boundary condition making conservative the kinetic–fluid coupling algorithm. Moreover, this kinetic scheme is a relaxation scheme (cf. [13]) which allows to obtain an entropic result for the resolution of the multispecies Euler system (cf. [19,20]).

The plan of this paper is the following: in Section 2, we recall the basic properties of the Wang Chang–Uhlenbeck equations (this section summarizes the paper [17]). In Section 3, we recall the energy relaxation and the kinetic schemes introduced in [13,14], and we extend these notions to the multispecies case. In Section 4, we describe the kinetic–fluid coupling algorithm, the boundary condition at the kinetic–fluid interface and the boundary condition – which is a Marshak condition – designed for the asymptotic matching of the fluid area with the uranium–iron source. At last, in Section 5, we present numerical results which show that the proposed kinetic–fluid coupling algorithm coupled with the asymptotic matching gives very good results.

2. The Wang Chang–Uhlenbeck equations and its fluid limit

In this section, we recall the system constituted with the Wang Chang–Uhlenbeck equations (cf. [2,3]) – which are semi-classical multispecies Boltzmann equations – and the fluid limit of these kinetic equations which is the hyperbolic multispecies Euler system closed with a non-classical state equation. This section summarizes the results written in [17].

In this paper, we use the following notations and definitions:

- k is the subscript of the kth species;
- $\overline{k}$ is the number of species in the gas mixture;
- $\epsilon_i^k \in \mathbb{R}^+$ is the value of the ith quantified energy level of the species k;
- $g_i^k \in \mathbb{N}$ is the degenerescency of the ith quantified energy level of the species k. The degenerescencies g_i^k are integers which define the dimension of the subspace associated to the eigenvalues ϵ_i^k of the quantic Hamiltonian operator of the Schrödinger equation, Hamiltonian describing the quantified electronic energy transitions in an atom of the species k;
- $f_i^k(t,x,v) \in \mathbb{R}^+$ is the distribution function of the species k at the ith quantified energy level;
- m_k is the atomic mass of the species k.

The variable $t \in \mathbb{R}^+$ is the time, $x \in \mathbb{R}^3$ and $v \in \mathbb{R}^3$ are, respectively, the position in the usual space and the microscopic velocity. Let us now define the macroscopic density ρ_k, the macroscopic velocity u_k and the macroscopic total energy E_k of the species k with

$$\begin{aligned}
\rho_k &= \sum_i \int_{\mathbb{R}^3} m_k f_i^k(v)\mathrm{d}v,\\
\rho_k u_k &= \sum_i \int_{\mathbb{R}^3} m_k v f_i^k(v)\,\mathrm{d}v,\\
\rho_k E_k &= \sum_i \int_{\mathbb{R}^3} m_k \left(\frac{1}{2}v^2 + \epsilon_i^k\right) f_i^k(v)\,\mathrm{d}v
\end{aligned} \tag{1}$$

and let us define the density ρ, the velocity u and the total energy E of the gas mixture, and the mass fraction Y_k of the species k with

$$\begin{aligned}
&\rho = \sum_k \rho_k \equiv \frac{1}{\tau},\\
&\rho u = \sum_k \rho_k u_k,\\
&\rho E = \sum_k \rho_k E_k \equiv \rho\left(\frac{u^2}{2} + \varepsilon\right),\\
&Y_k = \frac{\rho_k}{\rho} \in [0,1] \quad \left(\text{we see that } \sum_k Y_k = 1\right).
\end{aligned} \tag{2}$$

The quantities τ and ε are, respectively, the specific volume and the specific internal energy of the gas mixture.

2.1. The Wang Chang–Uhlenbeck equations

Let us consider a multispecies gas mixture whose distribution functions $f_i^k(t,x,v)$ are solution of the Wang Chang–Uhlenbeck equations (cf. [2,3])

$$\partial_t f_i^k + v\cdot\nabla_x f_i^k = Q_i^k(\{f_j^{k_*}\}_{j,k_*}), \tag{3}$$

where

$$Q_i^k = \sum_{j,h,l,k_*} Q_{i,j\to h,l}^{k,k_*}. \tag{4}$$

The operator $Q_{i,j\to h,l}^{k,k_*}$ is a *collision operator* describing a collision of a particle of the species k at the energy level i with a particle k_* at the energy level j, collision giving a particle of the species k at the energy level h and a particle k_* at the energy level l. The collision operator $Q_{i,j\to h,l}^{k,k_*}$ is given by

$$Q_{i,j\to h,l}^{k,k_*} = \int_{\Delta_{i,j\to h,l}^{k,k_*}(v)} \left[f_h^k(v') f_l^{k_*}(v_*') \frac{g_i^k g_j^{k_*}}{g_h^k g_l^{k_*}} - f_i^k(v) f_j^{k_*}(v_*)\right] \mathscr{B}_{i,j\to h,l}^{k,k_*}(v, v_*, \Omega)\,\mathrm{d}v_*\,\mathrm{d}\Omega. \tag{5}$$

The positive function $\mathscr{B}_{i,j\to h,l}^{k,k_*}(v, v_*, \Omega)$ is the collision kernel and will be defined below and Ω is a vector of the unit sphere $\mathscr{S}^2$. The couple of velocities (v, v_*) and (v', v_*') are, respectively, the pre-collision and the post-collision velocities; they are related through

$$\begin{aligned}
&v' = v_g + \Omega\frac{\sqrt{2}\mu_{kk_*}}{m_k}\sqrt{\frac{1}{2}|v-v_*|^2 + \Delta\epsilon_{i,j\to h,l}^{k,k_*}},\\
&v_*' = v_g - \Omega\frac{\sqrt{2}\mu_{kk_*}}{m_{k_*}}\sqrt{\frac{1}{2}|v-v_*|^2 + \Delta\epsilon_{i,j\to h,l}^{k,k_*}},\\
&v_g \equiv \frac{m_k v + m_{k_*} v_*}{m_k + m_{k_*}},
\end{aligned} \tag{6}$$

where

$$\Delta\epsilon_{i,j\to h,l}^{k,k_*} = \frac{m_k}{\mu_{kk_*}}\left(\epsilon_i^k - \epsilon_h^k\right) + \frac{m_{k_*}}{\mu_{kk_*}}\left(\epsilon_j^{k_*} - \epsilon_l^{k_*}\right) \tag{7}$$

with the reduced mass $\mu_{kk_*} = m_k m_{k_*}/(m_k + m_{k_*})$. Thus, the integration set $\Delta^{k,k_*}_{i,j\to h,l}(v)$ in (5) is defined by

$$\Delta^{k,k_*}_{i,j\to h,l}(v) = \mathscr{S}^2 \times \left\{ v_* \in \mathbb{R}^3 \text{ such that } \tfrac{1}{2}|v - v_*|^2 + \Delta\epsilon^{k,k_*}_{i,j\to h,l} \geqslant 0 \right\}.$$

The relations (6) are equivalent to the kinematic relations of a microscopic inelastic collision that is to say to the relations:

$$m_k v + m_{k_*} v_* = m_k v' + m_{k_*} v'_*, \tag{8a}$$

$$m_k \tfrac{v^2}{2} + m_k \epsilon^k_i + m_{k_*} \tfrac{v_*^2}{2} + m_{k_*} \epsilon^{k_*}_j = m_k \tfrac{v'^2}{2} + m_k \epsilon^k_h + m_{k_*} \tfrac{v'^2_*}{2} + m_{k_*} \epsilon^{k_*}_l. \tag{8b}$$

The relation (8a) supposes that the two particles which collide together define an isolated system; the relation (8b) characterizes the conservation of the total microscopic energy before and after the collision, this microscopic energy being the sum of a classical part – i.e., $m_k \frac{v^2}{2}$ – and of a non-classical or quantic part – i.e., $m_k \epsilon^k_i$: that is why we also name *semi-classical Boltzmann operator* the Wang Chang–Uhlenbeck operator (5).

The collision kernel $\mathscr{B}^{k,k_*}_{i,j\to h,l}(v, v_*, \Omega)$ is defined by

$$\mathscr{B}^{k,k_*}_{i,j\to h,l}(v, v_*, \Omega) = |v - v_*| \cdot \sigma^{k,k_*}_{i,j\to h,l}(v, v_*, \Omega),$$

where $\sigma^{k,k_*}_{i,j\to h,l}(v, v_*, \Omega)$ is the microscopic cross-section of the collision $(v, i), (v_*, j) \to (v', h), (v'_*, l)$.

The cross-section $\sigma^{k,k_*}_{i,j\to h,l}$ must be related to $\sigma^{k,k_*}_{h,l\to i,j}$ through

$$g^k_i g^{k_*}_j \sigma^{k,k_*}_{i,j\to h,l}(v, v_*, \Omega) \cdot |v - v_*| \, \mathrm{d}v \, \mathrm{d}v_* \, \mathrm{d}\Omega = g^k_h g^{k_*}_l \sigma^{k,k_*}_{h,l\to i,j}(v', v'_*, \Omega') \cdot |v' - v'_*| \, \mathrm{d}v' \, \mathrm{d}v'_* \, \mathrm{d}\Omega', \tag{9}$$

which is derived from the quantic Fermi's golden rule (for classical collisions, the relation which is equivalent to (9) is derived from the Liouville's theorem).

A particular class of cross-sections model verifying (9) is the Anderson's one proposed in [5]. This model is defined by

$$\sigma^{k,k_*}_{i,j\to h,l}(v, v_*, \Omega) = \sigma^{k,k_*}_0 \cdot p^{k,k_*}_{i,j\to h,l}(v, v_*) \tag{10}$$

with

$$p^{k,k_*}_{i,j\to h,l}(v, v_*) = \frac{g^k_h g^{k_*}_l \cdot \left(\frac{1}{2}|v - v_*|^2 + \Delta\epsilon^{k,k_*}_{i,j\to h,l} \right)}{\sum_{\oplus m,n} g^k_m g^{k_*}_n \cdot \left(\frac{1}{2}|v - v_*|^2 + \Delta\epsilon^{k,k_*}_{i,j\to m,n} \right)}, \tag{11}$$

$\sigma^{k,k_*}_0 = \sigma^{k_*,k}_0$ being a strictly positive constant. The notation $\oplus m, n$ in (11) means that m and n are chosen in the sum when $\frac{1}{2}|v - v_*|^2 + \Delta\epsilon^{k,k_*}_{i,j\to m,n}$ is positive (we recall that $\Delta\epsilon^{k,k_*}_{i,j\to h,l}$ is defined by (7)).

Here, $p^{k,k_*}_{i,j\to h,l}(v, v_*) \in [0, 1]$ – which verifies $\sum_{h,l} p^{k,k_*}_{i,j\to h,l}(v, v_*) = 1$ – defines the (conditional) probability transition from a given quantic electronic metastable state (i, j) to the quantic electronic metastable state (h, l) for the species k and k_* knowing the velocities v and v_*.

Let us remark that when we decide to "forget" the existence of quantic electronic metastable states in the atoms, it means that we impose $\Delta\epsilon^{k,k_*}_{i,j\to h,l} = 0$ and $g^k_i = g^k_h$ for each (i, j, h, l, k, k_*) (each electronic state is supposed to be indiscernable from an other electronic state in that case). And, it is easy to prove that $f^k = \sum_i f^k_i$ is solution of the classical multispecies Boltzmann equations associated to the hard sphere model whose the constant cross-sections are equal to σ^{k,k_*}_0.

This remark shows that the Anderson's model is interesting when it is possible to consider the atoms globally as hard spheres because it needs only to have an estimation of the cross-section σ^{k,k_*}_0 to define

$\sigma^{k,k_*}_{i,j\to h,l}(v,v_*,\Omega)$ (the complicated electronic structure of atoms with high atomic number makes very difficult to have a theoretical or experimental evaluation of each $\sigma^{k,k_*}_{i,j\to h,l}(v,v_*,\Omega)$). In that situation, we can define σ^{k,k_*}_0 with

$$\sigma^{k,k_*}_0 = \pi\cdot(r_k + r_{k_*})^2, \tag{12}$$

where r_k is the radius of an atom of the species k considered as a hard sphere. For AVLIS applications, experimental results (cf. [4]) and ab initio simulations show that an atom of uranium can be considered as a hard sphere with radius equal to 2.43 Å; similarly, an atom of iron can be considered as a hard sphere with radius equal to 1.53 Å.

The Anderson's model was experimentally justified in [7] and is used in Monte-Carlo simulations for AVLIS applications (see [5,6,8]): in the numerical results of Section 5, we will used this cross-sections model.

2.2. Convergence toward a Maxwellian equilibrium and fluid limit

In this section, we describe without proof the basic properties of the Wang Chang–Uhlenbeck equations (3). The proof are written in [17].

2.2.1. Convergence toward a Maxwellian equilibrium

We have the following result:

Lemma 2.1. *Let us suppose that the cross-sections* $\sigma^{k,k_*}_{i,j\to h,l}(v,v_*,\Omega)$ *verifies* (9). *Then*:

$$\forall(i,k):\quad Q^k_i = 0 \iff \exists(\{Y_k>0\}_k,\rho>0,u,T>0) \text{ such that } \forall(i,k):\ f^k_i(v) = \mathscr{M}^k_i(v),$$

where $\mathscr{M}^k_i(v)$ *is the Maxwellian defined by*

$$\mathscr{M}^k_i(v) = \frac{Y_k}{m_k}\cdot\frac{\rho}{\left(2\pi\frac{T}{m_k}\right)^{3/2}}\cdot\frac{g^k_i}{\mathscr{Z}_k(T)}\cdot\exp\left[-m_k\frac{\frac{1}{2}(v-u)^2+\epsilon^k_i}{T}\right], \tag{13}$$

$\mathscr{Z}_k(T) = \sum_i g^k_i\exp(-\frac{m_k\epsilon^k_i}{T})$ *being the partition function of the species* k.

And by using the previous lemma with the classical H-theorem, we obtain:

Lemma 2.2. *Let us suppose that the cross-sections* $\sigma^{k,k_*}_{i,j\to h,l}(v,v_*,\Omega)$ *verifies* (9) *and that* $f^k_i(t,v)$ *is solution of the spatially homogeneous Wang Chang–Uhlenbeck equations* (3) *which means that*

$$\partial_t f^k_i(t,v) = Q^k_i(\{f^{k_*}_j\}_{j,k_*}).$$

Then, we have

$$\forall(i,k):\quad \lim_{t\to+\infty}\|f^k_i - \mathscr{M}^k_i\|_{L_1} = 0.$$

2.2.2. Fluid limit

Let us now define the internal energy

$$\mathscr{E}\left(Y_1,\ldots,Y_{\overline{k}-1},T\right) = E - \tfrac{1}{2}u^2 \tag{14}$$

with

$$\mathscr{E}\big(Y_1,\ldots,Y_{\overline{k-1}},T\big)=\sum_k Y_k\mathscr{E}_k(T), \tag{15a}$$

$$\mathscr{E}_k(T)=\mathscr{E}_k^{\mathrm{cl}}(T)+\mathscr{E}_k^{\mathrm{ncl}}(T), \tag{15b}$$

$$\mathscr{E}_k^{\mathrm{cl}}(T)=\frac{3}{2}\cdot\frac{T}{m_k}, \tag{15c}$$

$$\mathscr{E}_k^{\mathrm{ncl}}(T)=\frac{\sum_i g_i^k\epsilon_i^k\exp\big(-[m_k\epsilon_i^k/T]\big)}{\mathscr{Z}_k(T)}, \tag{15d}$$

where $\mathscr{Z}_k(T)=\sum_i g_i^k\exp(-[m_k\epsilon_i^k/T])$ is the partition function of the species k. The quantity T is the temperature of the mixture and $\{Y_k\}_k$ defines the mass fractions of the mixture. The energy $\mathscr{E}_k$ is the internal energy of the species k; $\mathscr{E}_k^{\mathrm{cl}}$ and $\mathscr{E}_k^{\mathrm{ncl}}$ are, respectively, the classical and the non-classical part of the internal energy $\mathscr{E}_k$ of the species k.

By using Lemma 2.1, we can formally derive the fluid limit of the Wang Chang–Uhlenbeck equations:

Property 2.1 (Fluid limit). *Let us suppose that the cross-sections* $\sigma_{i,j\to h,l}^{k,k_*}(v,v_*,\Omega)$ *verify* (9) *and the property*

$$\exists\lambda>0/\forall(v,v_*,\Omega,i,j,h,l,k,k_*):\quad \sigma_{i,j\to h,l}^{k,k_*}(v,v_*,\Omega)\simeq\frac{1}{\lambda} \tag{16}$$

and let us suppose that $f_i^k(t,x,v)$ *– which is now noted* $f_{i,\lambda}^k(t,x,v)$ *– is solution of the Wang Chang–Uhlenbeck equations* (3). *Moreover, let us define* $(\{Y_{k,\lambda}\}_k,\rho_\lambda,u_\lambda,E_\lambda)$ *with the relations* (1) *and* (2) *and let us suppose that*

$$\exists\big(\{Y_k\}_k,\rho,u,E\big)/\lim_{\lambda\to0}\big(\{Y_{k,\lambda}\}_k,\rho_\lambda,u_\lambda,E_\lambda\big)=\big(\{Y_k\}_k,\rho,u,E\big).$$

Then, we formally have that

$$\lim_{\lambda\to0}f_{i,\lambda}^k=\mathscr{M}_i^k \tag{17}$$

and that $(\{Y_k\}_k,\rho,u,E)$ *is solution of the hyperbolic multispecies Euler system*

$$\begin{aligned}&\forall k:\quad \partial_t(Y_k\rho)+\nabla_x\cdot(Y_k\rho u)=0,\\ &\partial_t(\rho u)+\nabla_x\cdot(\rho u\otimes u+P\overline{\overline{1}})=0,\\ &\partial_t(\rho E)+\nabla_x\cdot[(\rho E+P)u]=0\end{aligned} \tag{18}$$

with $E=\frac{1}{2}u^2+\varepsilon$, *system which is closed with the equations of state*

$$\begin{aligned}&\varepsilon=\mathscr{E}\big(Y_1,\ldots,Y_{\overline{k-1}},T\big)\quad(\text{cf. (15)}),\\ &\tau P=T\sum_k\frac{Y_k}{m_k}.\end{aligned} \tag{19}$$

Moreover, the system (18) *and* (19) *admits the specific entropy* $s(Y_1,\ldots,Y_{\overline{k-1}},\tau,\varepsilon)$ *defined by*

$$s\big(Y_1,\ldots,Y_{\overline{k-1}},\tau,\varepsilon\big)=\sum_k Y_k s_k(Y_k,\tau,T), \tag{20a}$$

$$s_k(Y_k,\tau,T) = -\frac{1}{m_k}\left[\log\tau + \frac{3}{2}\log\left(\frac{T}{m_k}\right) + \log\left(\mathscr{Z}_k(T)\right) + \frac{\varepsilon_k^{\mathrm{ncl}}(T)}{T/m_k} - \log\left(\frac{Y_k}{m_k}\right)\right], \tag{20b}$$

where the temperature T is solution of $\mathscr{E}(Y_1,\ldots,Y_{\overline{k-1}},T) = \varepsilon$ with $\varepsilon = E - \frac{1}{2}u^2$ ($\tau \equiv \frac{1}{\rho}$ is the specific volume), entropy which is associated to the entropy flux $\rho u \cdot s$ and which is a strictly convex function of the variables τ and ε.

The system (18) and (19) is the multispecies Euler system closed with a non-classical state equation, and defines the *fluid limit* of the Wang Chang–Uhlenbeck equations.

The property (16) is important: it supposes that there is only one microscopic time scale; if it was not the case, there would be different relaxation time scales and the fluid limit could be more complicated (in (16), λ is proportional to the mean collision time and to the mean free path of the gas mixture). Let us note that the Anderson's model (10) and (11) verifies the property (16) as soon as it exists $\sigma_0 > 0$ such that $\mathscr{C}(\sigma_0^{k,k_*}) = \sigma_0$ for any (k,k_*), which is the case in AVLIS applications: indeed, the radius of uranium and iron atoms are of the same order (they are, respectively, equal to 2.43 and 1.53 Å); then, the relation (12) allows to conclude.

Of course, the proof of Property 2.1 is formal and an exact proof is still an open problem. Let us just remark that from a theoretical point of view, we should precise in Property 2.1 the physical domain $\mathscr{D}$ with the boundary condition on $\partial\mathscr{D}$ where the Wang Chang–Uhlenbeck equations (3) are solved. Indeed, the convergence result (17) could be false near $\partial\mathscr{D}$ where it could appear kinetic boundary layers (the Knudsen layer is a good example, see Section 4.3). Thus, the result of Property 2.1 has to be seen as a result which is "almost true" in $\mathscr{D}$.

Let us note that we can write for each species k

$$s_k(Y_k,\tau,T) = s_k^{\mathrm{cl}}(\tau_k,T) + s_k^{\mathrm{ncl}}(T) \tag{21}$$

by defining the partial entropies s_k^{cl} and s_k^{ncl}, respectively, associated to the classical part $\varepsilon_k^{\mathrm{cl}} = \mathscr{E}_k^{\mathrm{cl}}(T_k)$ and to the non-classical part $\varepsilon_k^{\mathrm{ncl}} = \mathscr{E}_k^{\mathrm{ncl}}(T_k)$ of the internal energy $\mathscr{E}_k$ of the species k (cf. (15b)–(15d)). These partial entropies are given by

$$s_k^{\mathrm{cl}}(\tau_k,T_k) = -\frac{1}{m_k}\left[\log(m_k\tau_k) + \frac{3}{2}\log\left(\frac{T_k}{m_k}\right)\right] \tag{22}$$

(knowing that $Y_k\tau_k = \tau$) and by

$$s_k^{\mathrm{ncl}}(T_k) = -\frac{1}{m_k}\left[\log(\mathscr{Z}_k(T_k)) + \frac{\varepsilon_k^{\mathrm{ncl}}(T_k)}{T_k/m_k}\right]. \tag{23}$$

Moreover, the entropy s verifies the second thermodynamic principle

$$-T\,\mathrm{d}s = \mathrm{d}\mathscr{E} + P\,\mathrm{d}\tau$$

when $\forall k:\ \mathrm{d}Y_k = 0$.

Finally, let us remark that (19) is equivalent to

$$\mathscr{E}\left(Y_1,\ldots,Y_{\overline{k-1}},T_1,\ldots,T_{\overline{k}}\right) = \sum_k Y_k\mathscr{E}_k(T_k)$$

with $\mathscr{E}_k(T_k)$ given by (15b)–(15d) and with

$$\begin{aligned}
&\forall (k,l): \quad T_k = T_l \quad \text{(isothermal law)},\\
&P = \sum_k P_k \quad \text{(Dalton law)},\\
&\forall k: \quad Y_k \tau_k = \tau \quad \text{(mixture law)},\\
&\forall k: \quad \tau_k P_k = \frac{T_k}{m_k} \quad \text{(equations of state)}.
\end{aligned} \tag{24}$$

3. Relaxation schemes for the multispecies Euler system

In this section, we propose a class of entropic schemes for the previous hyperbolic multispecies Euler system (18)

$$\begin{aligned}
&\forall k: \quad \partial_t(Y_k\rho) + \nabla_x \cdot (Y_k \rho u) = 0,\\
&\partial_t(\rho u) + \nabla_x \cdot (\rho u \otimes u + P\overline{\overline{1}}) = 0,\\
&\partial_t(\rho E) + \nabla_x \cdot [(\rho E + P)u] = 0
\end{aligned} \tag{25}$$

($E = \frac{1}{2}u^2 + \varepsilon$) closed with the equations of state

$$\begin{aligned}
&\varepsilon = \mathscr{E}\big(Y_1, \ldots, Y_{\overline{k-1}}, T\big),\\
&P = \mathscr{P}(Y_1, \ldots, Y_{\overline{k-1}}, \rho, T) \equiv \sum_k P_k(Y_k\rho, T),\\
&P_k(\rho_k, T_k) = \rho_k \frac{T_k}{m_k},
\end{aligned} \tag{26}$$

$\mathscr{E}(Y_1, \ldots, Y_{\overline{k-1}}, T) = \sum_k Y_k \mathscr{E}_k(T)$ being defined by (15b)–(15d). This class of entropic schemes extends the notion of *energy relaxation schemes* initially proposed in [13] and recalled below. Let us remark that this entropic property is a strong stability property which induces that the scheme preserves the positivity of the mass fractions, density, pressure and internal energy, and that the shocks, if they exist, are entropic; nevertheless, this last property is of no use in AVLIS applications since there are no shocks but only expansions (see Section 5).

Let us recall that the system (25) and (26) is the fluid limit of the Wang Chang–Uhlenbeck equations (3), is hyperbolic and admits the convex entropy $s(Y_1, \ldots, Y_{\overline{k}}, \tau, \varepsilon)$ given by

$$s\big(Y_1, \ldots, Y_{\overline{k-1}}, \tau, \varepsilon\big) = \sum_k Y_k s_k(Y_k, \tau, T), \tag{27a}$$

$$s_k(Y_k, \tau, T) = -\frac{1}{m_k}\left[\log \tau + \frac{3}{2}\log\left(\frac{T}{m_k}\right) + \log\left(\mathscr{Z}_k(T)\right) + \frac{\varepsilon_k^{\mathrm{ncl}}(T)}{T/m_k} - \log\left(\frac{Y_k}{m_k}\right)\right] \tag{27b}$$

and associated to the entropy flux $\rho u \cdot s$, see Property 2.1.

In this paper, we impose that the equations of state are given by (26) since one of the aims of this study is to couple the Wang Chang–Uhlenbeck equations (3) with its fluid limit. Moreover, to simplify the results and notations, we suppose now that the number of species is equal to two and we do not describe in detail all the properties and proof. Nevertheless, we generalize and we precise in [19] (see also [20]) all the properties described below for any number of species and for any equations of state admitting a thermodynamic entropy.

After, we will derive a particular class of relaxation schemes for the resolution of the multispecies Euler system (25) and (26) – namely the *kinetic schemes* – which will allow us to recover in a quite different way an entropic result initially proposed in [16]. These kinetic schemes will be used in the following section to couple the fluid domain with the kinetic domain.

In the following section, we briefly recall the basic properties of the energy relaxation schemes introduced in [13] and the basic properties of the kinetic schemes introduced in [14].

3.1. The energy relaxation schemes and the kinetic schemes

3.1.1. The energy relaxation schemes

The aim of this class of schemes proposed in [13] is to describe a general way to obtain entropic schemes for the resolution of the classical Euler system

$$\begin{aligned}
&\partial_t \rho + \nabla_x \cdot (\rho u) = 0,\\
&\partial_t (\rho u) + \nabla_x \cdot \left(\rho u \otimes u + P\overline{\overline{1}}\right) = 0,\\
&\partial_t (\rho E) + \nabla_x \cdot [(\rho E + P)u] = 0
\end{aligned} \tag{28}$$

for any state equations $\varepsilon(\tau, P)$ associated to a thermodynamic entropy by introducing relaxation terms (we recall that $\tau \equiv 1/\rho$).

For that purpose, let us choose a state equation $\varepsilon_a(\tau, P_a)$ more simple than the original state equation $\varepsilon(\tau, P)$ – for example, as the perfect gas equation of state – and let us define the energy relaxed system

$$\partial_t \rho + \nabla_x \cdot (\rho u) = 0, \tag{29a}$$

$$\partial_t (\rho u) + \nabla_x \cdot \left(\rho u \otimes u + P_a\overline{\overline{1}}\right) = 0, \tag{29b}$$

$$\partial_t (\rho E_a) + \nabla_x \cdot [(\rho E_a + P_a)u] = \frac{1}{\lambda}[\varepsilon_b - \mathscr{F}(\tau, \varepsilon_a)], \tag{29c}$$

$$\partial_t (\rho \varepsilon_b) + \nabla_x \cdot (\rho u \varepsilon_b) = -\frac{1}{\lambda}[\varepsilon_b - \mathscr{F}(\tau, \varepsilon_a)] \tag{29d}$$

with $E_a \equiv \frac{u^2}{2} + \varepsilon_a$ and where the energy $\mathscr{F}(\tau, \varepsilon_a)$ is such that

$$\varepsilon_a(\tau, P) + \mathscr{F}[\tau, \varepsilon_a(\tau, P)] = \varepsilon(\tau, P) \tag{30}$$

(the function $\mathscr{F}$ exists and is unique as soon as we suppose that ε and ε_a are such that $\partial_P \varepsilon > 0$ and $\partial_{P_a} \varepsilon_a > 0$). Let us define $E \equiv E_a + \varepsilon_b$. Then, the important characteristic of the system (29a)–(29d) is that it formally converges to the system (28) when λ goes to zero. In fact, it is possible to show that under some constraints, in particular on the choice of the state equation $\varepsilon_a(\tau, P_a)$, the formal first-order asymptotic equilibrium system of the relaxed system (29a)–(29d) is given by

$$\begin{aligned}
&\partial_t \rho + \nabla_x \cdot (\rho u) = 0,\\
&\partial_t (\rho u) + \nabla_x \cdot \left(\rho u \otimes u + P\overline{\overline{1}}\right) = \lambda \nabla_x (\mu \nabla_x \cdot u),\\
&\partial_t (\rho E) + \nabla_x \cdot [(\rho E + P)u] = \lambda \nabla_x \cdot (\mu u \nabla_x \cdot u)
\end{aligned}$$

where the viscosity μ is a positive function of the thermodynamic variables (see [13]). This property means that to obtain a numerical schemes for (28), we can discretize (29a)–(29d) by making λ go to zero. The

scheme is based on a splitting between the hyperbolic terms and the relaxation terms (n is the time subscript):

Hyperbolic stage. From an initial condition (ρ^n, u^n, E^n) and knowing ε_a^n, ε_b^n and P_a^n (which is equal to P^n), we solve on a spatial mesh and on a time step Δt the system

$$\partial_t \rho + \nabla_x \cdot (\rho u) = 0, \tag{31a}$$

$$\partial_t (\rho u) + \nabla_x \cdot \left(\rho u \otimes u + P_a \overline{\overline{1}} \right) = 0, \tag{31b}$$

$$\partial_t (\rho E_a) + \nabla_x \cdot [(\rho E_a + P_a) u] = 0, \tag{31c}$$

$$\partial_t (\rho \varepsilon_b) + \nabla_x \cdot (\rho u \varepsilon_b) = 0. \tag{31d}$$

Then, we obtain $(\rho^{n+1/2}, u^{n+1/2}, E_a^{n+1/2}, \varepsilon_b^{n+1/2})$ in each spatial mesh.

Energy relaxation stage. To obtain $(\rho^{n+1}, u^{n+1}, E^{n+1})$, we solve from the initial condition $(\rho^{n+1/2}, u^{n+1/2}, E_a^{n+1/2}, \varepsilon_b^{n+1/2})$ in each spatial mesh the spatially homogeneous system

$$\begin{aligned} &\partial_t \rho = 0, \\ &\rho \partial_t u = 0, \\ &\rho \partial_t E_a = \frac{1}{\lambda} [\varepsilon_b - \mathscr{F}(\tau, \varepsilon_a)], \\ &\rho \partial_t \varepsilon_b = -\frac{1}{\lambda} [\varepsilon_b - \mathscr{F}(\tau, \varepsilon_a)] \end{aligned} \tag{32}$$

with the same time step Δt and with $\lambda \to 0$. It induces that

$$\begin{aligned} &\rho^{n+1} = \rho^{n+1/2}, \\ &u^{n+1} = u^{n+1/2}, \\ &E^{n+1} = E_a^{n+1/2} + \varepsilon_b^{n+1/2}. \end{aligned}$$

Afterwards, we deduce ε_a^{n+1} and ε_b^{n+1} such that $E^{n+1} - (u^{n+1})^2/2 = \varepsilon_a^{n+1} + \varepsilon_b^{n+1}$ and $\varepsilon_b^{n+1} = \mathscr{F}(1/\rho^{n+1}, \varepsilon_a^{n+1})$. And, due to the relation (30), we obtain that $P_a^{n+1} = P^{n+1}$ (the equilibrium is indeed an *isobare equilibrium*).

An immediate property of the energy relaxation scheme is that, if we know a solver for the Euler system (31a)–(31c) associated to the equation of state $\varepsilon_a(\tau, P_a)$, it is easy to deduce a solver for the Euler system (28) associated to the equation of state $\varepsilon(\tau, P)$ without doing new developments. Let us note that a natural choice is to take $\varepsilon_a(\tau, P_a) = \tau P_a/(\gamma_a - 1)$, where $\gamma_a > 1$.

At last, it is also possible to show that this energy relaxation scheme has entropic properties (cf. [13,18]).

The aim of this section is to obtain numerical schemes for the resolution of the multispecies Euler system (25) and (26) with a similar relaxation technique and having similar entropic properties for the mixture entropy (27a) and (27b).

3.1.2. The kinetic schemes for any state equation

In this section, we briefly show that the kinetic schemes introduced by Perthame in [14] for a monospecies perfect gas (with $\gamma \in]1, 3]$) can be assimilated to a particular energy relaxation scheme when they are applied to any state equation: this remark was already written in [15].

To simplify the notation, we now suppose that the geometry is monodimensional Cartesian. The subscript i and n are, respectively, the space and time subscripts of the mesh $\{x_i\}$ and of the time sequence $\{t_n\}$;

$\Delta x_i \equiv x_{i+1/2} - x_{i-1/2}$ and $\Delta t \equiv t_{n+1} - t_n$ are, respectively, the space and time steps. The numerical scheme to solve (28) closed with the equation of state $\varepsilon(\tau, P)$ is defined by the conservative scheme

$$\begin{aligned}
\rho_i^{n+1/2} &= \rho_i^n - \frac{\Delta t}{\Delta x}(\mathfrak{I}_{i+1/2}^n - \mathfrak{I}_{i-1/2}^n),\\
(\rho u)_i^{n+1/2} &= (\rho u)_i^n - \frac{\Delta t}{\Delta x}(\wp_{i+1/2}^n - \wp_{i-1/2}^n),\\
(\rho E)_i^{n+1/2} &= (\rho E)_i^n - \frac{\Delta t}{\Delta x}(\aleph_{i+1/2}^n - \aleph_{i-1/2}^n).
\end{aligned} \tag{33}$$

In this section, the atomic mass of the monospecies gas is noted m.

Kinetic schemes for a perfect gas with $\gamma = 3$. We now suppose that $\varepsilon(\tau, P) = \tau P/(\gamma - 1)$ with $\gamma = 3$. The derivation of the kinetic schemes for a perfect gas with $\gamma = 3$ is based on the following lemma (cf. [14] and in [22, Lemma 7.3, p. 285]):

Lemma 3.1 (B. Perthame). *Let us define the initial conditions $\rho(0,x)$, $u(0,x)$ and $E(0,x)$ of the Euler system* (28) *which are supposed to be regular and let us define the function $\chi(v_x) \geqslant 0$ such that*

$$\begin{aligned}
&\int_{\mathbb{R}} (1, v_x^2)\chi(v_x)\,\mathrm{d}v_x = (1,1),\\
&\chi(-v_x) = \chi(v_x).
\end{aligned} \tag{34}$$

Let $h(t,x,v_x)$ be solution of the pure transport equation

$$\begin{aligned}
&\partial_t h + v_x \partial_x h = 0,\\
&h(t=0,x,v_x) = \mathbf{M}(x,v_x),
\end{aligned} \tag{35}$$

where

$$\mathbf{M}(x,v_x) = \frac{\rho(0,x)/m}{\sqrt{P(0,x)/\rho(0,x)}}\chi\left(\frac{v_x - u(0,x)}{\sqrt{P(0,x)/\rho(0,x)}}\right)$$

with $P(0,x)$ such that $\varepsilon(\tau,P) = \tau P/2$ (m is the atomic mass). Then, $\rho(t,x)$, $u(t,x)$ and $E(t,x)$ defined by

$$\begin{aligned}
\rho(t,x) &= \int_{\mathbb{R}} m h(t,x,v_x)\,\mathrm{d}v_x,\\
\rho(t,x)u(t,x) &= \int_{\mathbb{R}} m v_x h(t,x,v_x)\,\mathrm{d}v_x,\\
\rho(t,x)E(t,x) &= \int_{\mathbb{R}} m\frac{v_x^2}{2} h(t,x,v_x)\,\mathrm{d}v_x
\end{aligned}$$

is an approximation in Δt^2 of the solution of (28) *when $t < \Delta t$ (in 1D Cartesian geometry).*

Thus, by using an upwind scheme to solve (35) and by taking $\chi(v_x) = \frac{1}{\sqrt{2\pi}}\exp(-v_x^2/2)$, we obtain a *first order* numerical scheme for the monospecies Euler system (28) closed with the equation of state $\varepsilon(\tau,P) = \tau P/2$, the numerical fluxes being defined by

$$\begin{pmatrix} \mathfrak{I} \\ \wp \\ \aleph \end{pmatrix}_{i+1/2} = \begin{pmatrix} \mathfrak{I} \\ \wp \\ \aleph \end{pmatrix}_{i+1/2}^{+} + \begin{pmatrix} \mathfrak{I} \\ \wp \\ \aleph \end{pmatrix}_{i+1/2}^{-} \tag{36}$$

where the positive and negative half fluxes are given by

$$\begin{pmatrix} \mathfrak{I} \\ \wp \\ \aleph \end{pmatrix}^{+}_{i+1/2} = \int_{v_x>0} mv_x \begin{pmatrix} 1 \\ v_x \\ v_x^2 \end{pmatrix} \mathbf{M}(\rho_i, u_i, P_i)(v_x)\,\mathrm{d}v_x \tag{37}$$

and by

$$\begin{pmatrix} \mathfrak{I} \\ \wp \\ \aleph \end{pmatrix}^{-}_{i+1/2} = \int_{v_x<0} mv_x \begin{pmatrix} 1 \\ v_x \\ v_x^2 \end{pmatrix} \mathbf{M}(\rho_{i+1}, u_{i+1}, P_{i+1})(v_x)\,\mathrm{d}v_x, \tag{38}$$

$\mathbf{M}(\rho, u, P)(v_x)$ being the classical monodimensional Maxwellian

$$\mathbf{M}(\rho, u, P)(v_x) = \frac{\rho/m}{\sqrt{2\pi P/\rho}} \exp\left[-\frac{(v_x - u)^2}{P/\rho} \right]. \tag{39}$$

The important property of this scheme is that it is possible to prove that it is positive and entropic under a classical CFL criterion (cf. [16]). The formulas giving the numerical fluxes $\mathfrak{I}$, $\wp$ and $\aleph$ are given in Appendix A.

Kinetic schemes for a real gas. By using the technique of the energy relaxation scheme previously recalled, it is easy to extend the kinetic schemes to any state equation. Indeed, let us define ε_a with

$$\varepsilon_a(\tau, P) = \frac{\tau P}{2}$$

and let us note

$$\varepsilon_b(\tau, P) = \varepsilon(\tau, P) - \varepsilon_a(\tau, P). \tag{40}$$

Let us now solve (31a)–(31c) with the kinetic scheme described before: then, the numerical fluxes $(\mathfrak{I}, \wp, \aleph_a)$ are given by (36)–(38), and Eq. (31d) is solved with the kinetic scheme

$$(\rho\varepsilon_b)_i^{n+1} = (\rho\varepsilon_b)_i^n - \frac{\Delta t}{\Delta x}(\aleph_{b,i+1/2}^n - \aleph_{b,i-1/2}^n)$$

with $\aleph_{b,i+1/2}^n = \aleph_{b,i+1/2}^{n,+} + \aleph_{b,i+1/2}^{n,-}$,

$$\aleph_{b,i+1/2}^{n,+} \equiv \varepsilon_{b,i}^n \cdot \mathfrak{I}_{i+1/2}^{n,+} \quad \text{and} \quad \aleph_{b,i+1/2}^{n,-} \equiv \varepsilon_{b,i+1}^n \cdot \mathfrak{I}_{i+1/2}^{n,-}.$$

By noting that (cf. Appendix A)

$$\aleph_{a,i+1/2}^{+} = \frac{P_i u_i}{4} \mathscr{G}\left(-\sqrt{\frac{3}{2}} M_{a,i} \right) + E_{a,i} \cdot \mathfrak{I}_{i+1/2}^{+}$$

and that

$$\aleph_{a,i+1/2}^{-} = \frac{P_{i+1} u_{i+1}}{4} \mathscr{G}\left(\sqrt{\frac{3}{2}} M_{a,i+1} \right) + E_{a,i+1} \cdot \mathfrak{I}_{i+1/2}^{-}$$

($M_a \equiv u/\sqrt{3P/\rho}$ is the Mach number associated to $\varepsilon_a(\tau, P_a) = \tau P_a/2$ and $\mathscr{G}(x)$ is defined in the Appendix A), we easily find that the kinetic scheme obtained in that way can be written with (33), where the formulas giving the numerical fluxes $\mathfrak{I}$, $\wp$ and $\aleph$ considered as functions of ρ, u, P and E are *exactly* the same as

those obtained when the gas is supposed to be a perfect gas with $\gamma = 3$, formulas already given in Appendix A.

Thus, the kinetic schemes allow us to obtain general formulas for any state equation to define the numerical fluxes. Moreover, we could prove, as in the case of a perfect gas with $\gamma = 3$, that this kinetic scheme is positive under a classical CFL condition for any state equation $\varepsilon(\tau, P)$ as soon as $\varepsilon_a(\tau, P)$ is chosen such that $\varepsilon_b(\tau, P) > 0$. We could also prove that when the equation of state is of the form $\varepsilon(\tau, P) = \mathscr{E}^{\mathrm{cl}}(T) + \mathscr{E}^{\mathrm{ncl}}(T)$, where $\mathscr{E}^{\mathrm{cl}}(T)$ and $\mathscr{E}^{\mathrm{ncl}}(T)$ are defined by (15c) and (15d) and where $\tau P = T/m$, the kinetic scheme is entropic for the entropy s defined by (27b) under a classical CFL criterion, see [16].

3.2. The relaxation schemes applied to the resolution of the multispecies Euler system

We now apply the previous ideas in the case of the multispecies Euler system (25) and (26). The results proposed here are generalized in [20] (see also [19]) to other equations of state and to non-miscible fluid mixtures.

The central idea is to artificially "separate" each species by supposing that each vector $(\rho_k, \rho_k u_k, \rho_k E_k)$ of the species k is solution of the *monospecies* Euler system

$$\begin{aligned} &\partial_t \rho_k + \nabla_x \cdot (\rho_k u_k) = 0, \\ &\partial_t (\rho_k u_k) + \nabla_x \cdot \left(\rho_k u_k \otimes u_k + P_k \overline{\overline{1}} \right) = 0, \\ &\partial_t (\rho_k E_k) + \nabla_x \cdot [(\rho_k E_k + P_k) u_k] = 0 \end{aligned} \tag{41}$$

closed with the equations of state

$$\begin{aligned} &\varepsilon_k = \mathscr{E}_k(T_k) \quad (\text{cf. (15b)}), \\ &P_k(\rho_k, T) = \rho_k \frac{T}{m_k}. \end{aligned} \tag{42}$$

The variables ρ_k, u_k, $E_k \equiv \frac{u_k^2}{2} + \varepsilon_k$, P_k and T_k are, respectively, the density, the velocity, the total energy, the pressure and the temperature of the species k. A corollary of Property 2.1 is that each system (41) and (42) is hyperbolic and that

$$s_k(\tau_k, \varepsilon_k) = s_k^{\mathrm{cl}}(\tau_k, T_k) + s_k^{\mathrm{ncl}}(T_k) \tag{43}$$

with

$$s_k^{\mathrm{cl}}(\tau_k, T_k) = -\frac{1}{m_k} \left[\log(m_k \tau_k) + \frac{3}{2} \log\left(\frac{T_k}{m_k} \right) \right] \tag{44}$$

and

$$s_k^{\mathrm{ncl}}(T_k) = -\frac{1}{m_k} \left[\log(\mathscr{Z}_k(T_k)) + \frac{\varepsilon_k^{\mathrm{ncl}}(T_k)}{\frac{T_k}{m_k}} \right] \tag{45}$$

is a thermodynamic entropy associated to the entropy flux $\rho_k u_k \cdot s_k$. The partial entropies s_k^{cl} and s_k^{ncl} are, respectively, associated to the energies $\varepsilon_k^{\mathrm{cl}} = \mathscr{E}_k^{\mathrm{cl}}(T_k)$ and $\varepsilon_k^{\mathrm{ncl}} = \mathscr{E}_k^{\mathrm{ncl}}(T_k)$ given by (15c) and (15d).

Since the fluid limit (25) and (26) of the Wang Chang–Uhlenbeck equations (3) imposes that the mixture is an isothermal mixture (i.e., $T_1 = T_2$), we couple the two systems (41) ($k = 1$ and $k = 2$) with a relaxation term proportional to $(T_2 - T_1)$ to force the two systems to relax toward an isothermal equilibrium; in the same way, we relax the systems (41) with a relaxation term proportional to $(u_2 - u_1)$ to force the two systems to relax toward an isovelocity equilibrium.

Indeed, we propose the following relaxed system

$$\partial_t \rho_1 + \nabla_x \cdot (\rho_1 u_1) = 0, \tag{46a}$$

$$\partial_t (\rho_1 u_1) + \nabla_x \cdot \left(\rho_1 u_1 \otimes u_1 + P_1 \overline{\overline{1}} \right) = \frac{1}{\lambda}(u_2 - u_1), \tag{46b}$$

$$\partial_t (\rho_1 E_1) + \nabla_x \cdot [(\rho_1 E_1 + P_1) u_1] = \frac{1}{\lambda}(T_2 - T_1) + \frac{1}{\lambda} U_{\text{inter}}(u_2 - u_1), \tag{46c}$$

$$\partial_t \rho_2 + \nabla_x \cdot (\rho_2 u_2) = 0, \tag{46a$'$}$$

$$\partial_t (\rho_2 u_2) + \nabla_x \cdot \left(\rho_2 u_2 \otimes u_2 + P_2 \overline{\overline{1}} \right) = \frac{1}{\lambda}(u_1 - u_2), \tag{46b$'$}$$

$$\partial_t (\rho_2 E_2) + \nabla_x \cdot [(\rho_2 E_2 + P_2) u_2] = \frac{1}{\lambda}(T_1 - T_2) + \frac{1}{\lambda} U_{\text{inter}}(u_1 - u_2), \tag{46c$'$}$$

where

$$U_{\text{inter}} \in [\min(u_1, u_2), \max(u_1, u_2)].$$

We name *interfacial velocity* the velocity U_{inter} by analogy with the multiphasic Euler system (cf. [23]); λ is a strictly positive parameter (for example, λ^{-1} is proportional to $(\rho_1 + \rho_2)v$, where v is a strictly positive frequency): we formally see that the relaxation terms force the temperatures and the velocities of each species to relax to the same values, and that the more λ is important, the less the system (46a)–(46c′) converges to the *isothermal–isovelocity equilibrium*.

Let us note that the system (46a)–(46c′) is hyperbolic since the hydrodynamic transport for the species 1 and the hydrodynamic transport for the species 2 are coupled through the relaxation terms and not through differential terms.

3.2.1. Asymptotic analysis of the relaxed system

Of course, in order to have a system (46a)–(46c′) well posed, it is important that the *isothermal–isovelocity equilibrium* would be a stable equilibrium. We have the following result whose proof is presented in [20]:

Theorem 3.1. *The formal first-order asymptotic equilibrium system of the relaxed system* (46a)–(46c′) *is given by the system*

$$\begin{aligned}
&\partial_t (Y_1 \rho) + \nabla_x \cdot (Y_1 \rho u) = \nabla_x \cdot (\lambda J_1), \\
&\partial_t (Y_2 \rho) + \nabla_x \cdot (Y_2 \rho u) = \nabla_x \cdot (\lambda J_2), \\
&\partial_t (\rho u) + \nabla_x \cdot (\rho u \otimes u + P \overline{\overline{1}}) = \nabla_x (\lambda \mu \nabla_x \cdot u), \\
&\partial_t (\rho E) + \nabla_x \cdot [(\rho E + P) u] = \nabla_x \cdot [\lambda (h_1 J_1 + h_2 J_2)] + \nabla_x \cdot (\lambda \mu u \nabla_x \cdot u)
\end{aligned} \tag{47}$$

closed with the state equation (26) *and with*

$$\begin{aligned}
&J_1 = -J_2 = \rho Y_1 Y_2 (Y_2 \nabla_x P_1 - Y_1 \nabla_x P_2), \\
&h_k = \varepsilon_k + P_k / (Y_k \rho)
\end{aligned}$$

and where the viscosity μ is defined by

$$\mu(Y_1,\rho,T)=\frac{Y_1^2Y_2^2\rho^2T}{(Y_1(\mathrm{d}\mathscr{E}_1(T)/\mathrm{d}T)+Y_2(\mathrm{d}\mathscr{E}_2(T)/\mathrm{d}T))^2}\left(\frac{\mathrm{d}\mathscr{E}_1(T)/\mathrm{d}T}{m_2}-\frac{\mathrm{d}\mathscr{E}_2(T)/\mathrm{d}T}{m_1}\right)^2.$$

We see that the viscosity μ is positive and will be equal to zero when:

- $Y_1=0$ or $Y_1=1$, i.e., when the mixture is pure. Let us remark that, in that case, we have also $J_k=0$;
- when $m_1\mathrm{d}\mathscr{E}_1(T)/\mathrm{d}T=m_2\mathrm{d}\mathscr{E}_2(T)/\mathrm{d}T$: this is the case when the species 1 and 2 are identical that is to say when the mixture is again pure.

Let us note that the fluxes J_k can be rewritten with

$$J_k=D_{12}(P,C_1)\left[\nabla_xC_k+\left(1-\frac{m_k}{m}\right)C_k\frac{\nabla_xP}{P}\right], \tag{48}$$

where $D_{12}(P,C_1)$ is a positive function and where C_k is the molar fraction of the species k in the mixture defined by $C_k=Y_km/m_k$, m being equal to $(Y_1/m_1+Y_2/m_2)^{-1}$. We recognize in (48) the Fick law and the baro-diffusive effect which are classical diffusion processes.

This theorem shows that, near the equilibrium, the system (46a)–(46c′) is similar to a multispecies Navier–Stokes system which formally converges to the multispecies Euler system (25) when λ goes to zero.

3.2.2. Definition of the relaxation scheme and entropic result

To obtain a numerical scheme for the multispecies Euler system (25) and (26), we discretize the system (46a)–(46c′) by making λ go to zero to force the *isothermal–isovelocity equilibrium*. The numerical resolution of (46a)–(46c′) is based on a splitting between the hyperbolic terms and the relaxation terms (n is the time subscript):

- *Hyperbolic stage*. From an initial condition (Y_1^n,ρ^n,u^n,E^n) and knowing P_1^n, P_2^n and T^n, we solve on the spatial mesh $\{x_i\}$ and on a time step Δt the independent systems (41) for $k=1$ and $k=2$. Thus, we obtain $(Y_k^{n+1/2},\rho^{n+1/2},u_k^{n+1/2},E_k^{n+1/2})$ in each spatial mesh x_i.
- *Relaxation stage*. To obtain $(Y_1^{n+1},\rho^{n+1},u^{n+1},E^{n+1})$, we relax on the same time step Δt the system to the *isothermal–isovelocity equilibrium* from the initial condition $(Y_k^{n+1/2},\rho^{n+1/2},u_k^{n+1/2},E_k^{n+1/2})$ by solving in each spatial mesh

$$\partial_tY_1=0,$$

$$\partial_t\rho=0,$$

$$Y_1\rho\partial_tu_1=\frac{1}{\lambda}(u_2-u_1),$$

$$Y_1\rho\partial_tE_1=\frac{1}{\lambda}(T_2-T_1)+\frac{1}{\lambda}U_{\mathrm{inter}}(u_2-u_1),$$

$$Y_2\rho\partial_tu_2=\frac{1}{\lambda}(u_1-u_2),$$

$$Y_2\rho\partial_tE_2=\frac{1}{\lambda}(T_1-T_2)+\frac{1}{\lambda}U_{\mathrm{inter}}(u_1-u_2)$$

with $\lambda \to 0$ (we recall that $Y_2 = 1 - Y_1$). Thus, we have

$$\begin{aligned}
\rho^{n+1} &= \rho_1^{n+1/2} + \rho_2^{n+1/2},\\
Y_1^{n+1} &= \rho_1^{n+1/2}/\rho^{n+1},\\
u^{n+1} &= Y_1^{n+1/2} u_1^{n+1/2} + Y_2^{n+1/2} u_2^{n+1/2},\\
E^{n+1} &= Y_1^{n+1/2} E_1^{n+1/2} + Y_2^{n+1/2} E_2^{n+1/2}.
\end{aligned}$$

And the pressures P_1^{n+1}, P_2^{n+1} and the temperature T^{n+1} are such that

$$\begin{aligned}
&Y_1^{n+1} \mathscr{E}_1(T^{n+1}) + Y_2^{n+1} \mathscr{E}_2(T^{n+1}) = E^{n+1} - \frac{(u^{n+1})^2}{2},\\
&P_1^{n+1} = Y_1^{n+1} \rho^{n+1} \frac{T^{n+1}}{m_1},\\
&P_2^{n+1} = Y_2^{n+1} \rho^{n+1} \frac{T^{n+1}}{m_2}
\end{aligned}$$

(we easily verify that $E^{n+1} - \frac{(u^{n+1})^2}{2} > 0$ as soon as $\varepsilon_1^{n+1/2} > 0$ and $\varepsilon_2^{n+1/2} > 0$, and thus as soon as each hyperbolic stage is positive).

The main result of this section is the following:

Theorem 3.2. *Let us suppose that each numerical scheme used to discretize each hyperbolic step* (41) *and* (42) *is entropic. Thus, the relaxation scheme defined before and used to discretize the multispecies Euler system* (25) *and* (26) *is entropic.*

The proof is based on the fact that the entropy mixture $s(Y_1, \tau, \varepsilon)$ given by (27a) and (27b) is the solution of a minimization problem similar to the one of the Gibbs theorem coming from the kinetic theory (cf. [18,20]).

This result – which is very general in fact (cf. [20]) and not only true for the equations of state (26) – shows that we do not have to construct new solvers to obtain an entropic scheme for the multispecies Euler system (25) and (26) as soon as entropic solvers are known for each monospecies Euler system (41) and (42). In the following section, we propose a particular class of these relaxation schemes – the *kinetic schemes* – and, by using Theorem 3.2, we will recover an entropic result for the kinetic schemes applied to the multispecies Euler system (25) and (26), result previously proposed in [16].

3.3. The kinetic schemes applied to the resolution of the multispecies Euler system

We define the (explicit) kinetic scheme for the hyperbolic step (41) and (42) with

$$\rho_{k,i}^{n+1/2} = \rho_{k,i}^n - \frac{\Delta t}{\Delta x}(\mathfrak{I}_{k,i+1/2}^n - \mathfrak{I}_{k,i-1/2}^n), \tag{49a}$$

$$(\rho_k u_k)_i^{n+1/2} = (\rho_k u_k)_i^n - \frac{\Delta t}{\Delta x}(\wp_{k,i+1/2}^n - \wp_{k,i-1/2}^n), \tag{49b}$$

$$(\rho_k E_k)_i^{n+1/2} = (\rho_k E_k)_i^n - \frac{\Delta t}{\Delta x}(\aleph_{k,i+1/2}^n - \aleph_{k,i-1/2}^n), \tag{49c}$$

where the numerical fluxes $(\mathfrak{I}_k, \wp_k, \aleph_k)$ are the kinetic fluxes defined in Appendix A. Then, by using Theorem 3.2, we easily obtain the following proposition already obtained in [16] with another technique (although we use one of the results proposed in [16], see the proof below):

Proposition 3.1. *Let us suppose that the equations of state are defined by* (26). *Then, the kinetic scheme defined by*

$$\begin{aligned}
&\forall k: \quad (Y_k\rho)_i^{n+1} = (Y_k\rho)_i^n - \frac{\Delta t}{\Delta x}(\mathfrak{I}_{k,i+1/2}^n - \mathfrak{I}_{k,i-1/2}^n),\\
&(\rho u)_i^{n+1} = (\rho u)_i^n - \frac{\Delta t}{\Delta x}(\wp_{i+1/2}^n - \wp_{i-1/2}^n),\\
&(\rho E)_i^{n+1} = (\rho E)_i^n - \frac{\Delta t}{\Delta x}(\aleph_{i+1/2}^n - \aleph_{i-1/2}^n),
\end{aligned} \tag{50}$$

where the numerical fluxes are given by

$$\begin{aligned}
&\wp = \sum_k \wp_k,\\
&\aleph = \sum_k \aleph_k
\end{aligned} \tag{51}$$

is entropic under a classical CFL criterion for the specific entropy s defined by (27a) *and* (27b) *and associated to the entropy flux* $\rho u \cdot s$.

Proof of Proposition 3.1. We know that the monospecies kinetic scheme (49a)–(49c) is entropic under a classical CFL criterion for the entropy s_k given by (27b) (with $\tau = Y_k\tau_k$): this result is shown in [16]. Then, we deduce the result by applying Theorem 3.2 and by summing each Eq. (49b) and each Eq. (49c) together knowing that $k = 1, \ldots, \overline{k}$. □

4. Kinetic–fluid coupling and the Marshak condition for the multispecies Euler system

The aim of this section is to propose for the simulation of the gas mixture expansion of the AVLIS process an algorithm of domain decomposition to couple the resolution of the Wang Chang–Uhlenbeck equations (3) in the kinetic area and the resolution of the multispecies Euler system (25) and (26) in the fluid area, the scheme used to discretize the Euler system being the kinetic scheme proposed in the previous section.

Let us remark that the uranium–iron expansion is stationary: thus, the expansion has to be described by the stationary solution of the Wang Chang–Uhlenbeck equations (3) and by the stationary solution of the Euler system (25) and (26) in the kinetic and fluid areas.

This coupling technique was previously used in [11] to couple the classical monospecies Boltzmann equation with the classical monospecies Euler system for aerodynamic problems. It uses *half flux conditions* to define the boundary condition at the kinetic–fluid interface. These conditions come from a kinetic interpretation of the Euler equations and give formulas for the numerical fluxes at the kinetic–fluid interface similar to those obtained with the kinetic schemes presented in the previous section: that is why we will use the kinetic schemes to solve the multispecies Euler system in the fluid domain although we could *a priori* use any good scheme designed for the multispecies Euler system apart from the meshes which have a frontier with the kinetic–fluid interface.

In this section, we use the following definitions and notations (*see the Fig.* 2):

- The physical domain $\mathscr{D} \subset \mathbb{R}^3$ is constituted of the kinetic domain $\mathscr{K} \subset \mathbb{R}^3$ – where the mean free path is important – and of the fluid domain $\mathscr{F} \subset \mathbb{R}^3$ – where the mean free path is tiny. We have $\mathscr{D} = \mathscr{K} \cup \mathscr{F}$ and the kinetic–fluid interface $\mathscr{I}$ is defined by $\mathscr{I} = \mathscr{K} \cap \mathscr{F}$. The kinetic–fluid coupling algorithm proposed in this section supposed no overlapping between $\mathscr{K}$ and $\mathscr{F}$: thus, $\mathscr{I}$ is a surface (or a line if $\mathscr{D} \subset \mathbb{R}^2$ and points if $\mathscr{D} \subset \mathbb{R}$).

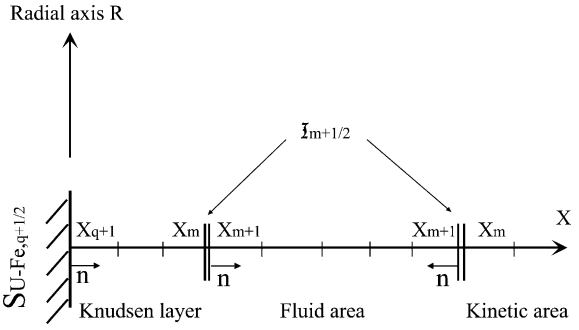

Fig. 2. Structure of a plume created by evaporation.

- The boundary condition for the kinetic domain $\mathscr{K}$ at the interface $\mathscr{I}$ is noted $\Gamma_{\text{fluid}\to\text{kinetic}}(\mathscr{I})$; conversely, for the fluid domain $\mathscr{F}$, it is noted $\Gamma_{\text{kinetic}\to\text{fluid}}(\mathscr{I})$. These boundary conditions will be defined below.
- A mesh of the kinetic domain $\mathscr{K}$ having a frontier on the kinetic–fluid interface $\mathscr{I}$ is noted X_m; this frontier is noted $\mathscr{I}_{m+1/2}$ and the fluid mesh having also this interface on its frontier is noted X_{m+1}. The distribution function f_i^k in the mesh X_m is noted $f_i^k(x_m, v)$.
- The uranium–iron emission surface is noted $\mathscr{S}_{\text{U–Fe}}$ and the meshes having a frontier on $\mathscr{S}_{\text{U–Fe}}$ are noted X_{q+1}, this frontier being noted $\mathscr{S}_{\text{U–Fe},q+1/2}$. Of course, we have $\mathscr{S}_{\text{U–Fe},q+1/2} \subset \mathscr{S}_{U-Fe} \subset \partial\mathscr{D}$.

We recall that i is the subscript of the ith quantified energy level of the species k, see the notations at the beginning of Section 2.

Let us note that the feature of the gas expansion in the AVLIS process is completely similar to the feature of the gas expansion in the coma of a comet (cf. [9]) and to the feature of the gas expansion of a volcanic jet when the atmosphere of the planet is rarefied (cf. [10]): thus, all the techniques and results of this section can be applied to the problems exposed in [9,10].

4.1. Algorithm of the kinetic–fluid coupling

The algorithm is the following (we will explicitly define the boundary conditions $\Gamma_{\text{fluid}\to\text{kinetic}}(\mathscr{I})$ and $\Gamma_{\text{kinetic}\to\text{fluid}}(\mathscr{I})$ in the following section):

Initialisation of the fluid domain $\mathscr{F}$ and of the boundary condition $\Gamma_{fluid\to kinetic}(\mathscr{I})$. We solve the pure transport equations $\partial_t f_i^k + v\cdot\nabla_x f_i^k = 0$ in the domain $\mathscr{D}$ to obtain the stationary solution without collisions in $\mathscr{D}$. Then, we initialize the fluid domain $\mathscr{F}$ which allows us to define the boundary condition $\Gamma_{\text{fluid}\to\text{kinetic}}(\mathscr{I})$ on the kinetic–fluid interface $\mathscr{I}$. This stage does not take a lot of CPU time since we do not take into account the Wang Chang–Uhlenbeck operators (4) and (5).

First stage: computation of the kinetic domain $\mathscr{K}$. Knowing the boundary condition $\Gamma_{\text{fluid}\to\text{kinetic}}(\mathscr{I})$, we solve the Wang Chang–Uhlenbeck equations (3) in the kinetic domain $\mathscr{K}$. Then, we compute the boundary condition $\Gamma_{\text{kinetic}\to\text{fluid}}(\mathscr{I})$ at the interface $\mathscr{I}$ for the fluid domain $\mathscr{F}$ after having done enough collisions to obtain a stationary solution of the Wang Chang–Uhlenbeck equations in $\mathscr{K}$.

Second stage: computation of the fluid domain $\mathscr{F}$. Knowing the boundary condition $\Gamma_{\text{kinetic}\to\text{fluid}}(\mathscr{I})$ at the kinetic–fluid interface $\mathscr{I}$, we solve the multispecies Euler system (25) and (26) with the kinetic scheme (50) and (51) in the fluid domain $\mathscr{F}$. Then, we compute the new boundary condition $\Gamma_{\text{fluid}\to\text{kinetic}}(\mathscr{I})$ at the interface $\mathscr{I}$ for the kinetic domain $\mathscr{K}$ when we have reached a stationary solution of the Euler system in $\mathscr{F}$.

Third stage: convergence of the algorithm? We stop the algorithm if the global level of convergence is enough; if not, we come back to the *first stage*.

Let us note that the existence of a proof of the convergence of this algorithm is an open problem, even for simplified kinetic models. Nevertheless, the numerical results obtained in Section 5 seem to state that there is convergence.

4.2. Boundary condition at the kinetic–fluid interface

Since we solve the fluid limit of the Wang Chang–Uhlenbeck equations (3) in the fluid domain $\mathscr{F}$, the kinetic–fluid interface $\mathscr{I}$ has to be placed in an area which is at the thermodynamic equilibrium which means that the solution f_i^k of the Wang Chang–Uhlenbeck equations in $\mathscr{F}$ *without coupling* has to be a Maxwellian given by (13). Of course, since we do not know the solution of (3) in $\mathscr{D}$, we have to choose a priori the position of $\mathscr{F}$ in the domain $\mathscr{D}$ and, then, the position of the kinetic–fluid interface $\mathscr{I}$. Nevertheless, for AVLIS aplications, the domain $\mathscr{D}$ is fixed and we only modify the uranium–iron emission condition on $\mathscr{S}_{\text{U–Fe}}$ (this emission condition will be defined in Sections 4.3 and 5.2) which does not change to much the position of the fluid domain. Thus, for a given domain $\mathscr{D}$, the position of $\mathscr{I}$ can be chosen from a first simulation without kinetic–fluid coupling. Of course, a best way would be to find a criterion which would automatically estimate an a priori position of the kinetic–fluid interface $\mathscr{I}$ at the beginning of the kinetic–fluid algorithm.

To simplify the notations, we suppose in this section that the expansion is monodimensional in the x-direction: thus, the kinetic–fluid interface $\mathscr{I}$ is perpendicular to the x-direction and we only need to compute the fluxes of the Euler system in the x-direction. Moreover, we write in this paper the boundary condition only on the part of the interface $\mathscr{I}$ which verifies $n_x > 0$, where n is the normal on $\mathscr{I}$ entering the fluid domain $\mathscr{F}$ (see Fig. 2). The projection on the x-direction of the microscopic velocity v is noted v_x ($v \equiv (v_x, v_y, v_z) \in \mathbb{R}^3$).

Of course, it is easy to extend the proposed boundary condition for any geometry and any shape of the kinetic–fluid interface $\mathscr{I}$ (the numerical results in the following part are obtained for an axisymmetrical geometry and for an interface being parallel or perpendicular to the radial axis, see Fig. 4).

4.2.1. Boundary condition $\Gamma_{fluid\to kinetic}(\mathscr{I})$ on $\mathscr{I}_{m+1/2}$ for the Wang Chang–Uhlenbeck equations

After the *second stage* of the coupling algorithm, we know the stationary solution of the Euler system (25) and (26) and, thus, we know the mass fractions Y_k of each species k, the density ρ, the velocity u and the temperature T of the gas mixture in each fluid frontier mesh X_{m+1} – see Fig. 2 – at the time $t_n = +\infty$ (which defines the last time step of the numerical resolution of the Euler system). Because of the kinetic interpretation of the Euler system (25) and (26) (cf. Property 2.1), we now consider that the fluid domain $\mathscr{F}$ is an uranium–iron emission source for the kinetic domain $\mathscr{K}$ through each interface $\mathscr{I}_{m+1/2}$. Thus, since n_x is supposed to be positive, the boundary condition $\Gamma_{\text{fluid}\to\text{kinetic}}(\mathscr{I})$ on $\mathscr{I}_{m+1/2}$ for each species k are given by

$$f_i^k(x_{m+1/2}, v) \equiv \mathscr{M}_i^k(t_n = +\infty, x_{m+1}, v) \quad \text{if } v_x < 0, \tag{52}$$

where $\mathscr{M}_i^k$ is the Maxwellian defined by (13) that is to say by

$$\mathscr{M}_i^k(v) = \frac{Y_k}{m_k} \cdot \frac{\rho}{(2\pi(T/m_k))^{\frac{3}{2}}} \cdot \frac{g_i^k}{\mathscr{Z}_k(T)} \cdot \exp\left\{ - m_k \frac{\frac{1}{2}[(v_x - u)^2 + v_y^2 + v_z^2] + \epsilon_i^k}{T} \right\}, \tag{53}$$

with $(\rho, u, T) \equiv (\rho, u, T)_{x=x_{m+1}}$ (we recall that $u \in \mathbb{R}$ in that section).

4.2.2. Boundary condition $\Gamma_{kinetic\to fluid}(\mathscr{I})$ on $\mathscr{I}_{m+1/2}$ for the Euler system

After the *first stage* of the coupling algorithm, we know the kinetic solution $f_i^k(x_m, v)$ of (3) in each kinetic frontier mesh X_m. Thus, we can evaluate the macroscopic fluxes of mass $\mathfrak{I}_{k,m+1/2}^+$ for each species k, the macroscopic fluxes $\wp_{m+1/2}^+$ of the mixture momentum and the macroscopic fluxes $\aleph_{m+1/2}^+$ of the mixture

total energy which enter into the fluid mesh X_{m+1} through the interface $\mathscr{I}_{m+1/2}$. They are defined by the formulas (let us recall that we suppose that $n_x > 0$)

$$\begin{aligned}
\mathfrak{I}^+_{k,m+1/2} &= \sum_i \int\int\int_{v_x>0} m_k v_x f_i^k(x_m, v)\,\mathrm{d}v,\\
\wp^+_{m+1/2} &= \sum_{k,i} \int\int\int_{v_x>0} m_k v_x^2 f_i^k(x_m, v)\,\mathrm{d}v,\\
\aleph^+_{m+1/2} &= \sum_{k,i} \int\int\int_{v_x>0} m_k v_x \left(\frac{v^2}{2} + \epsilon_i^k\right) f_i^k(x_m, v)\,\mathrm{d}v.
\end{aligned} \tag{54}$$

Conversely, we know the value of the macroscopic fluxes which leave the fluid domain $\mathscr{F}$ at any time t_n of the numerical resolution of the Euler system since the distribution $f_i^k(t_n, x_{m+1}, v)$ in the fluid mesh X_{m+1} is the Maxwellian $\mathscr{M}_i^k(t_n, x_{m+1}, v)$ by hypothesis, Maxwellian given by (53). Then, using again the kinetic interpretation of the multispecies Euler system (cf. Property 2.1), we deduce that the boundary condition $\Gamma_{\text{kinetic}\to\text{fluid}}(\mathscr{I})$ on $\mathscr{I}_{m+1/2}$ associated to the kinetic scheme (50) and (51) – or to another good scheme – can be given by

$$\begin{aligned}
\mathfrak{I}_{k,m+1/2} &= \mathfrak{I}^+_{k,m+1/2} + \mathfrak{I}^{-,n}_{k,m+1/2},\\
\wp_{m+1/2} &= \wp^+_{m+1/2} + \wp^{-,n}_{m+1/2},\\
\aleph_{m+1/2} &= \aleph^+_{m+1/2} + \aleph^{-,n}_{m+1/2},
\end{aligned} \tag{55}$$

where the negative half fluxes $\mathfrak{I}^{-,n}_{k,m+1/2}$, $\wp^{-,n}_{m+1/2}$ and $\aleph^{-,n}_{m+1/2}$ are defined by (54) by replacing $v_x > 0$ and $f_i^k(x_m, v)$, respectively, with $v_x < 0$ and $\mathscr{M}_i^k(t_n, x_{m+1}, v)$. We easily see that the formulas giving $\mathfrak{I}^{-,n}_{k,m+1/2}$, $\wp^{-,n}_{m+1/2}$ and $\aleph^{-,n}_{m+1/2}$ are those giving the negative half fluxes of the kinetic schemes described in the previous section, the formulas are given in Appendix A.

Let us note that the boundary conditions (54) and (55) correspond to a Marshak condition which will be explicitly used in the following section to take into account the Knudsen layer effects in the numerical resolution of the multispecies Euler system. Moreover, we can see that the boundary condition (52) coupled with the boundary conditions (54) and (55) makes conservative the coupling algorithm proposed at Section 4.1.

Finally, let us recall that the Wang Chang–Uhlenbeck equations (3) are solved with a Monte-Carlo technique (cf. [5–8]). Then, to reduce the statistical noise in the computation of the quantities (54), we compute the half fluxes during each iteration of the Monte-Carlo algorithm of the *first stage* of the coupling algorithm by updating the statistic average of (54) as soon as a particle crosses the interface $\mathscr{I}_{m+1/2}$ to go into the fluid domain $\mathscr{F}$; afterwards, this particle is killed. Of course, if the numerical method to solve the Wang Chang–Uhlenbeck equations is a deterministic method, the quantities (54) is computed at the end of the first stage of the coupling algorithm.

4.3. Boundary condition in the Knudsen Layer for the Euler system

To obtain the gas expansion in the AVLIS process, an electronic beam heats the (liquid) surface $\mathscr{S}_{\text{U–Fe}} \subset \partial\mathscr{D}$ (cf. Section 1 and Fig. 1). Afterwards, the uranium–iron gas mixture expands in the physical domain $\mathscr{D}$ and condensates on $\partial\mathscr{D}$. Due to the interaction of the source $\mathscr{S}_{\text{U–Fe}}$ with this electronic beam, the distribution of each species k on the liquid surface $\mathscr{S}_{\text{U–Fe}}$ is given by distribution functions $\phi_i^k(v)$ which are physical data coming from experimental studies and modelization hypothesis (see Section 5.2): this means that the distribution functions of the evaporated particles are defined by $\phi_i^k(v)$ on $\mathscr{S}_{\text{U–Fe}}$, when $v \cdot n > 0$, where n is the normal on the source $\mathscr{S}_{\text{U–Fe}}$ entering in $\mathscr{D}$.

Moreover, we suppose that *near the source* $\mathscr{S}_{\text{U–Fe}}$, the evaporation problem is monodimensional in the direction orthogonal to the source $\mathscr{S}_{\text{U–Fe}}$, direction which is supposed to be x: thus, $\mathscr{S}_{\text{U–Fe}}$ is located by $x = 0$ as on Fig. 2.

4.3.1. Existence of a Knudsen layer and asymptotic matching

Near the surface $\mathscr{S}_{\text{U–Fe}}$, the mean free path is very tiny. Nevertheless, the gas mixture is not at the thermodynamic equilibrium because the distribution function $f_i^k(t, x = 0, v_x > 0) \equiv \phi_i^k(v)$ is imposed by the boundary condition on the source $\mathscr{S}_{\text{U–Fe}}$ which implies that $f_i^k(t, x = 0, v) \neq \mathscr{M}_i^k(v)$: the important consequence is that the Euler system (25) and (26) is not valid near the surface $\mathscr{S}_{\text{U–Fe}}$ (in other words, the formal convergence (17) of Property 2.1 is not valid on $\mathscr{S}_{\text{U–Fe}}$). Nevertheless, because of the collisions, the gas mixture recovers the thermodynamic equilibrium at a distance of some mean free paths from the surface $\mathscr{S}_{\text{U–Fe}}$ and the Euler system becomes valid: the area between the surface $\mathscr{S}_{\text{U–Fe}}$ and the place where the gas mixture recovers the thermodynamic equilibrium is named *Knudsen layer*, see Fig. 2.

Thus, we can summarize the expansion of the gas mixture in the AVLIS process with (see also the feature of the gas expansion in the coma of a comet in [9]):

$$\text{Evaporation from } \mathscr{S}_{\text{U–Fe}} \subset \partial\mathscr{D} \rightarrow \text{Knudsen layer} \rightarrow \text{Fluid domain } \mathscr{F} \rightarrow \text{Kinetic domain } \mathscr{K}$$
$$\text{i.e., rarefied area} \rightarrow \text{Condensation on } \partial\mathscr{D}.$$

To optimize the gain in CPU time and in required computer memory due to the kinetic–fluid coupling, we would like to take into account the effects of the Knudsen layer without solving the Wang Chang–Uhlenbeck equations in this layer but by asymptotically matching the fluid domain $\mathscr{F}$ on the surface $\mathscr{S}_{\text{U–Fe}}$: it can be done by using an ad hoc boundary condition on $\mathscr{S}_{\text{U–Fe}}$ for the multispecies Euler system.

More precisely, when the fluid domain $\mathscr{F}$ is asymptotically matched with the source $\mathscr{S}_{\text{U–Fe}}$, the multispecies Euler system (25) and (26) is solved in the mesh X_{q+1} although this mesh is inside the Knudsen layer (let us recall that X_{q+1} is a mesh of the physical domain $\mathscr{D}$ centered on x_{q+1} which has a frontier $\mathscr{S}_{\text{U–Fe},q+1/2} \subset \mathscr{S}_{\text{U–Fe}}$, see Fig. 2): then, to take into account the effect of the Knudsen layer in the mesh X_{q+1}, we have to find ad hoc values of the macroscopic fluxes $\mathfrak{I}_{k,q+1/2}$, $\wp_{q+1/2}$ and $\aleph_{q+1/2}$ on the interface $\mathscr{S}_{\text{U–Fe},q+1/2}$ in the numerical scheme (50). It can be done by studying the *half space problem* which will help us to define the *Marshak condition*.

4.3.2. The half space problem

To obtain this boundary condition, the best way is a priori to solve the monodimensional half space problem which is also called Milne's problem (a similar approach is proposed for semi-conductor problems where it could also exist a Knudsen layer, see [12]). Here, we rescale the Knudsen layer by writing that $x = 0$ corresponds to the uranium–iron evaporation source $\mathscr{S}_{\text{U–Fe}}$ and that $x = +\infty$ corresponds to the exit of the Knudsen layer, i.e., to the entry of the fluid domain $\mathscr{F}$. The half space problem is the following:

Does it exist $\{Y_k\}_k$, ρ, u *and* T *which define the Maxwellians* $\mathscr{M}_i^k(v)$ *given by (53) such that the problem*

$$\text{For all } (i,k): \quad \begin{cases} v \cdot \nabla_x f_i^k(x,v) = Q_i^k, \\ f_i^k(x = 0, v_x > 0) \equiv \phi_i^k(v), \\ f_i^k(x = +\infty, v) \equiv \mathscr{M}_i^k(v)_{x=+\infty} \end{cases} \tag{56}$$

is well posed.

Let us suppose that (56) is well posed: then, it would be possible to define a boundary condition on $x = 0$ for the multispecies Euler system (25) and (26) by imposing $(\{Y_k\}_k, \rho, u, T)_{x=0}$ with the moments of $\mathscr{M}_i^k(v)_{x=+\infty}$ given by the resolution of (56): this would correspond to the *asymptotic matching* of the fluid domain $\mathscr{F}$ on the surface $\mathscr{S}_{\text{U–Fe}}$.

In the case of a linearized classical monospecies Boltzmann operator, it is possible to obtain some theoretical results on the existence of a solution of (56). This solution is parametrized by the Mach number at $x = +\infty$ which has to be less than one (cf. [25]).

Some numerical experiments performed in [26] have proven the existence of a solution parametrized also by the Mach number at $x = +\infty$ for a monospecies BGK operator and when the boundary condition $f(x = 0, v_x > 0) \equiv \phi(v)$ is a classical centered Maxwellian $\mathscr{M}(v)$, Mach number which has to be less or equal than one.

For monospecies Boltzmann or BGK operators, a very simplified analytical approach is proposed in [27,28] when the boundary condition at $x = 0$ is a centered Maxwellian (the idea is to study (56) in the classical monospecies case by supposing that $\exists \beta > 0$ such that $f(x = 0, v_x < 0) = \beta \mathscr{M}(v)_{x=+\infty}$ and by taking the moments of (56)): the analytical formulas giving ρ, u and T at $x = +\infty$ are again parametrized by the Mach number at $x = +\infty$ which is also supposed to be less than or equal to one from physical considerations. The numerical results are very similar to those proposed in [26]. Let us note that these formulas are obtained for any $\gamma \in]1, 3]$; in [26], the results are obtained for a gas with $\gamma = 5/3$.

It is important to note that all these previous theoretical or numerical results can not be applied in our case for three reasons:

- the Wang Chang–Uhlenbeck operators (3) are not classical monospecies Boltzmann operators or BGK operators;
- in the case of a classical monospecies Boltzmann operator, the Mach number at $x = +\infty$ is a free parameter (which has to be subsonic). In some situation, it is possible to show that the exit of the Knudsen layer has to be sonic: then, the exit of the Knudsen layer is completely known; but, in other cases met in AVLIS expansions, it is impossible to know a priori the Mach number at the exit of the Knudsen layer (cf. [21]);
- the boundary condition $\phi_i^k(v)$ on the source $\mathscr{S}_{\text{U–Fe}}$ is not a Maxwellian because of the heating electronic beam (one of the uranium energy metastable level is excited, see Section 5.2): this makes much more difficult to obtain analytical results similar to those of [27,28].

Thus, we have to find another way to obtain the boundary condition for the multispecies Euler system at the source $\mathscr{S}_{\text{U–Fe}}$.

4.3.3. The Marshak condition for the Euler system coupled with a kinetic scheme

The Marshak condition was proposed in Los Alamos around the year 1940 for radiative transfer and neutron transport problems. Then, it was extended and justified in [24] to the gas dynamics equations to find boundary conditions for the asymptotic matching on a wall of the Navier–Stokes system and, then, to give slip boundary conditions: this gives Robin boundary conditions.

The Marshak condition. If we suppose that we can apply at $x = 0$ a Dirichlet condition in the case of the Euler system, the Marshak condition simply means that $(\{Y_k\}_k, \rho, u, T)_{x=0}$ is solution of the non-linear problem

$$\begin{aligned}
&\sum_i \int\int\int_{v_x>0} m_k v_x \mathscr{M}_i^k(v)_{x=0}\,\mathrm{d}v = \sum_i \int\int\int_{v_x>0} m_k v_x \phi_i^k(v)\,\mathrm{d}v \quad \text{for all } k \in \{1,\dots,\overline{k}\},\\
&\sum_{k,i} \int\int\int_{v_x>0} m_k v_x^2 \mathscr{M}_i^k(v)_{x=0}\,\mathrm{d}v = \sum_{k,i} \int\int\int_{v_x>0} m_k v_x^2 \phi_i^k(v)\,\mathrm{d}v,\\
&\sum_{k,i} \int\int\int_{v_x>0} m_k v_x \left(\frac{v^2}{2} + \epsilon_i^k\right) \mathscr{M}_i^k(v)_{x=0}\,\mathrm{d}v = \sum_{k,i} \int\int\int_{v_x>0} m_k v_x \left(\frac{v^2}{2} + \epsilon_i^k\right) \phi_i^k(v)\,\mathrm{d}v,
\end{aligned} \tag{57}$$

where the Maxwellian $\mathscr{M}_i^k(v)_{x=0}$ is defined by (53) with $(\{Y_k\}_k, \rho, u, T) \equiv (\{Y_k\}_k, \rho, u, T)_{x=0}$ (we recall that i is the ith electronic metastable energy level of the species k).

Coupling of the Marshak condition (57) *with a kinetic scheme*. We see that the difficulty is now to solve the non-linear problem (57); moreover, it is not obvious that a Dirichlet condition is a good boundary condition for the Euler system at the continuous level. To avoid these difficulties at the discrete level, we construct a ghost cell on the source $\mathscr{S}_{\text{U–Fe},q+1/2}$ defined by the solution of (57), and we apply the kinetic decomposition of the macroscopic fluxes on $\mathscr{S}_{\text{U–Fe},q+1/2}$ to obtain the (explicit) macroscopic numerical fluxes used to asymptotically match the fluid domain on the uranium–iron source $\mathscr{S}_{\text{U–Fe}}$. Then, $(\mathfrak{I}_k, \wp, \aleph)_{q+1/2}$ used in the numerical scheme (50) and (51) is given by

$$\begin{aligned}
\mathfrak{I}^n_{k,q+1/2} &= \mathfrak{I}^{\text{source}}_{k,q+1/2} + \mathfrak{I}^{-,n}_{k,q+1/2},\\
\wp^n_{q+1/2} &= \wp^{\text{source}}_{q+1/2} + \wp^{-,n}_{q+1/2},\\
\aleph^n_{q+1/2} &= \aleph^{\text{source}}_{q+1/2} + \aleph^{-,n}_{q+1/2},
\end{aligned} \tag{58}$$

with

$$\begin{aligned}
\mathfrak{I}^{\text{source}}_{k,q+1/2} &= \sum_i \int\int\int_{v_x>0} m_k v_x \phi^k_{i,q+1/2}(v)\,\mathrm{d}v,\\
\wp^{\text{source}}_{q+1/2} &= \sum_{k,i} \int\int\int_{v_x>0} m_k v_x^2 \phi^k_{i,q+1/2}(v)\,\mathrm{d}v,\\
\aleph^{\text{source}}_{q+1/2} &= \sum_{k,i} \int\int\int_{v_x>0} m_k v_x \left(\frac{v^2}{2}+\epsilon^k_i\right)\phi^k_{i,q+1/2}(v)\,\mathrm{d}v
\end{aligned} \tag{59}$$

and with

$$\begin{aligned}
\mathfrak{I}^{n,-}_{k,q+1/2} &= \sum_i \int\int\int_{v_x<0} m_k v_x \mathscr{M}^k_i(t_n, x_{q+1}, v)\,\mathrm{d}v,\\
\wp^{n,-}_{q+1/2} &= \sum_{k,i} \int\int\int_{v_x<0} m_k v_x^2 \mathscr{M}^k_i(t_n, x_{q+1}, v)\,\mathrm{d}v \equiv \sum_k \wp^{n,-}_{k,q+1/2},\\
\aleph^{n,-}_{q+1/2} &= \sum_{k,i} \int\int\int_{v_x<0} m_k v_x \left(\frac{v^2}{2}+\epsilon^k_i\right)\mathscr{M}^k_i(t_n, x_{q+1}, v)\,\mathrm{d}v \equiv \sum_k \aleph^{n,-}_{k,q+1/2}.
\end{aligned} \tag{60}$$

We can see that, *due to the kinetic decomposition of the macroscopic fluxes*, we do not have to solve the non-linear problem (57) and that this boundary condition is similar to the boundary condition on the kinetic–fluid interface $\mathscr{I}$ defined by (54) and (55).

The formulas giving $(\mathfrak{I}, \wp, \aleph)^{n,-}_{k,q+1/2}$ in (60) and considered as functions of $(\rho_k, u, P_k, E_k)^n_{q+1}$ are written in Appendix A.

The formulas giving (59) depend on the value of the distribution functions $\phi^k_i(v)$ which, in the AVLIS process, modelize the interaction between the source $\mathscr{S}_{\text{U–Fe}}$ and the heating electronic beam. If $\phi^k_i(v)$ are Maxwellians defined by (53), the formulas are again given in Appendix A.

Thus, the Marshak condition allows us to a priori take into account any emission condition $\phi^k_i(v)$, without postulating the value of the Mach number at the exit of the Knudsen layer and without doing any complicated analytical calculus: this technique is very *pragmatic* but gives *very good numerical results*.

For example, when the mesh size of the fluid domain is of the order of the mean free path, the macroscopic quantities found in the Knudsen layer by solving the Euler system with the asymptotic matching are almost equal to the macroscopic quantities given by the kinetic model; nevertheless, for a mesh size bigger than the mean free path, the results are of course less precise *but* are still very good, see the following part.

5. Application to the simulation of the Atomic Vapor Laser Isotopic Separation process

In this section, we apply the kinetic–fluid coupling technique proposed in the previous sections to simulate the expansion of the uranium–iron gas mixture in the AVLIS process, process which is described in Section 1 of this paper. The geometry is supposed to be axisymmetrical around the X-axis, the radial axis being noted R. Fig. 3 defines the physical domain $\mathscr{D}$ in that geometry.

Let us note that the Wang Chang–Uhlenbeck equations (3) are solved with the Monte-Carlo code presented in [6,7] whose algorithm is based on the Particle Test Monte-Carlo (PTMC) method and not on a classical Bird type method. Nevertheless, the choice of the Monte-Carlo technique used to solve the Wang Chang–Uhlenbeck equations does not interfere with the kinetic–fluid algorithm (more exactly, the boundary conditions (52), (53), (54) and (55) at the kinetic–fluid interface are independent of the Monte-Carlo algorithm) except for the gain in CPU time and in computer memory (see below).

At last, let us remark that the proposed kinetic–fluid coupling algorithm was tested with success in [21] in the case of a *monospecies perfect gas*, this simple configuration allowing to compare for example the proposed asymptotic matching in the Knudsen layer (see Section 4.3.3) with the asymptotic matching deduced from the numerical and analytical results of [26–28] (see also Section 4.3.2).

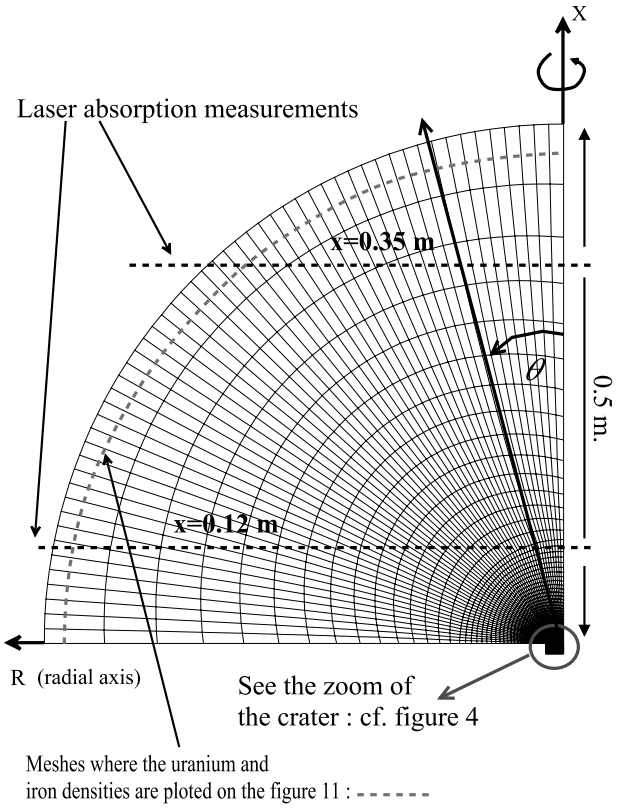

Fig. 3. Mesh of the physical domain (vacuum chamber, see Fig. 1).

5.1. The crater and the fluid domain $\mathscr{F}$

Fig. 4 is a zoom of the area where the uranium–iron is evaporated (see also Fig. 3): this area includes a *crater*; the boundary surface of this crater defines the source $\mathscr{S}_{\text{U–Fe}}$. This shape is due to the fact that the uranium–iron source is excavated by the impact of the electronic beam during the evaporation. The source $\mathscr{S}_{\text{U–Fe}}$, the Knudsen layer and the fluid domain $\mathscr{F}$ are included in the domain described in Fig. 4 (see also the simplified Fig. 2).

5.2. Emission conditions on the source $\mathscr{S}_{U–Fe}$

We suppose that the temperature T_s on the surface $\mathscr{S}_{\text{U–Fe}}$ is not uniform and divides the source $\mathscr{S}_{\text{U–Fe}}$ on three areas (cf. Fig. 4):

$$\begin{aligned}
&\text{for } r \leqslant R_1: \quad T_s(r) = 3400 \text{ K} \quad (R_1 = 0.85\ 10^{-2} \text{ m});\\
&\text{for } R_1 < r \leqslant R_2: \quad T_s(r) = 3200 \text{ K} \quad (R_2 = 1.7\ 10^{-2} \text{ m});\\
&\text{the last part of } \mathscr{S}_{\text{U–Fe}} \text{ is at the temperature } T_s(r) = 3000 \text{ K}.
\end{aligned} \tag{61}$$

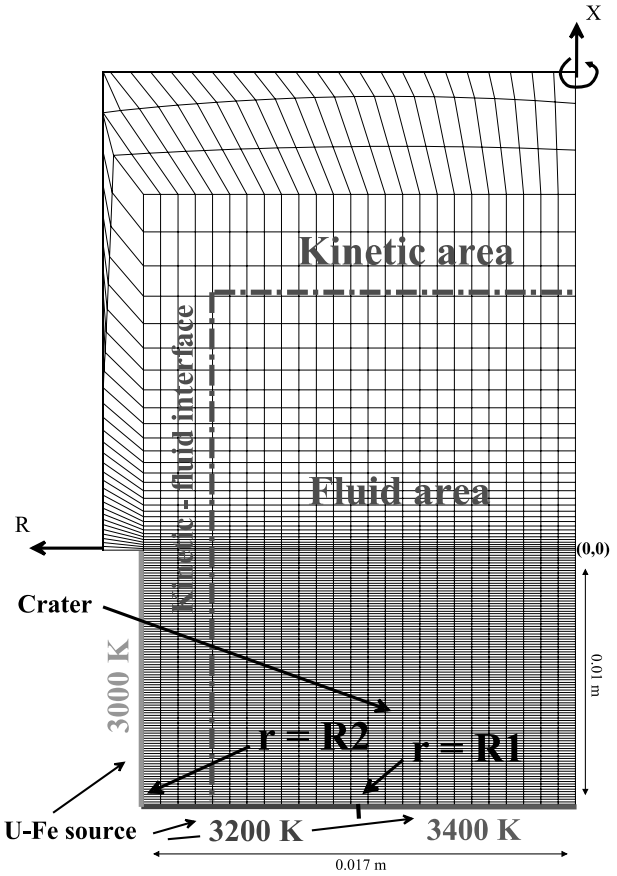

Fig. 4. Crater and kinetic–fluid interface.

This non-uniform temperature on $\mathscr{S}_{\mathrm{U-Fe}}$ is due to the presence of the electronic beam which only impacts the center of the crater (defined by $r \leqslant R_1$). Knowing these temperatures, we define the emission distribution functions $\phi_i^k(v)$ with:

For the uranium ($k \equiv {}^{238}\mathrm{U}$):

$$\phi_i^k(v) = C_{k,i}^{\mathrm{ste}}(T_s) \cdot n_s^k(T_s) \cdot \exp\left[-\frac{mv^2}{2T_s(r)} \right] \cdot g_i^k \exp\left(-\frac{m\epsilon_i^k}{T_s(r)} \right)$$
$$\text{if } i = 1 \text{ or } 2 \text{ and for all } r \geqslant 0; \text{ or if } i = 3 \text{ and } r > R_1; \tag{62a}$$

$$\phi_i^k(v) = C_{k,i}^{\mathrm{ste}}(T_s, T_*) \cdot n_s^k(T_s) \cdot \exp\left[-\frac{mv^2}{2T_s(r)} \right] \cdot g_i^k \exp\left(-\frac{m\epsilon_i^k}{T_*} \right) \quad \text{if } i = 3 \text{ and } r \leqslant R_1. \tag{62b}$$

The temperature T_* in (62b) will be defined in (64). Let us note that we can neglect the differences between the atomic masses and between the metastable energy levels of $^{235}\mathrm{U}$ and $^{238}\mathrm{U}$ for the simulation of the uranium gas expansion.

For the iron ($k \equiv \mathrm{Fe}$):

$$\phi_i^k(v) = C_{k,i}^{\mathrm{ste}}(T_s) \cdot n_s^k(T_s) \cdot \exp\left[-\frac{mv^2}{2T_s(r)} \right] \cdot g_i^k \exp\left(-\frac{m\epsilon_i^k}{T_s(r)} \right) \quad \text{if } i = 1 \text{ or } 2 \text{ and for all } r \geqslant 0. \tag{63}$$

The constants $C_{k,i}^{\mathrm{ste}}$ in (62a)–(63) are normalization constants easily deduced from (13). The density $n_s^k(T_s)$ in (62a) and (62b) is the vapor saturation density of the uranium on the surface $\mathscr{S}_{\mathrm{U-Fe}}$ at the temperature $T_s(r)$: it is given by a formula of the type Clausius–Clapeyron (see [29]); to simplify, the iron density $n_s^k(T_s)$ in (63) is supposed to be equal to 11.25% of the uranium density $n_s^k(T_s(r \leqslant R_1))$ in (62b).

Knowing the emission conditions (61)–(63), we can easily estimate the local mean free path of the gas mixture on the source $\mathscr{S}_{\mathrm{U-Fe}}$: it is between 10^{-5} and 10^{-4} m which induces a tiny local Knudsen number Kn ($Kn \in [10^{-3}, 10^{-2}]$). Moreover, we also deduce the evaporation rate which is equal to 3.7 kg/h for the uranium and to 0.2 kg/h for the iron.

The value of degenerescencies g_i^k and of metastable energy levels defined by $\epsilon_i^k \equiv \frac{\hbar}{m_k} \nu_i^k$ (m_k is the atomic mass and $\hbar$ is the Planck's constant: thus, ν_i^k is a frequency) are the followings:

For the uranium:

$$\begin{cases} g_1^k = 13, \\ g_2^k = 11, \\ g_3^k = 514 \end{cases} \quad \text{and} \quad \begin{cases} \nu_1^k = 0, \\ \nu_2^k = 620 \text{ cm}^{-1}, \\ \nu_3^k = 8338 \text{ cm}^{-1}. \end{cases}$$

For the iron:

$$\begin{cases} g_1^k = 9, \\ g_2^k = 26 \end{cases} \quad \text{and} \quad \begin{cases} \nu_1^k = 0, \\ \nu_2^k = 1466 \text{ cm}^{-1}. \end{cases}$$

In (62a)–(63), we only consider three metastable levels for the uranium and two metastable levels for the iron although the electronic structure of the uranium and of the iron is much more complicated: the last level (and its degenerescence) is an ad hoc average of the other metastable levels. Indeed, it is impossible to treat all the metastable levels for evident computer reasons; moreover, one of the most important informations that we want to know from the simulations is the number of uranium atoms at the second level ($\nu = 620$ cm^{-1}) compared to the number of uranium atoms at the first level which is the fundamental level ($\nu = 0$), this quantity being also deduced from experimental measures using laser absorption measurements (cf. Fig. 3): thus, we do not really need to know in detail the distribution functions of the uranium from the third metastable electronic energy level.

Moreover, the temperature T_* in (62b) modelizes the excitation of the uranium atoms because of the electronic beam which heats the center of the source $\mathscr{S}_{\text{U–Fe}}$ (the center is defined in (61) by $r \leqslant R_1$). This temperature is given by

$$T_* = C_* \cdot T_s(r \leqslant R_1), \tag{64}$$

where C_* is an excitation parameter deduced from experimental studies (let us recall that the temperature $T_s(r)$ of the source $\mathscr{S}_{\text{U–Fe}}$ is defined by (61)). Here, we choose $C_* = 1.7$ (we suppose that the iron is not excited by the electronic beam).

Let us note that the relations (61)–(64) are a simplified model which hides the difficulty to have an exact theoretical model of the interaction of the electronic beam with the source $\mathscr{S}_{\text{U–Fe}}$.

5.3. Numerical results

In this section, we compare the results obtained without kinetic–fluid coupling and the results obtained with the kinetic–fluid coupling algorithm presented in the previous part. We recall that the Wang Chang–Uhlenbeck equations (3) are solved with a Monte-Carlo technique.

5.3.1. Identical meshes with and without kinetic–fluid coupling

For Figs. 5–12, the physical mesh of $\mathscr{D}$ is defined in Figs. 3 and 4, and the size of the mesh is based on the local mean free path which is a priori estimated by using the emission conditions on the source $\mathscr{S}_{\text{U–Fe}}$. Below, we will take a bigger mesh in the fluid domain $\mathscr{F}$ for the kinetic–fluid coupling algorithm (cf. Figs. 13–15).

On Figs. 5–8, we can see the results with or without kinetic–fluid coupling in the crater for the axial and radial velocities of the gas mixture.

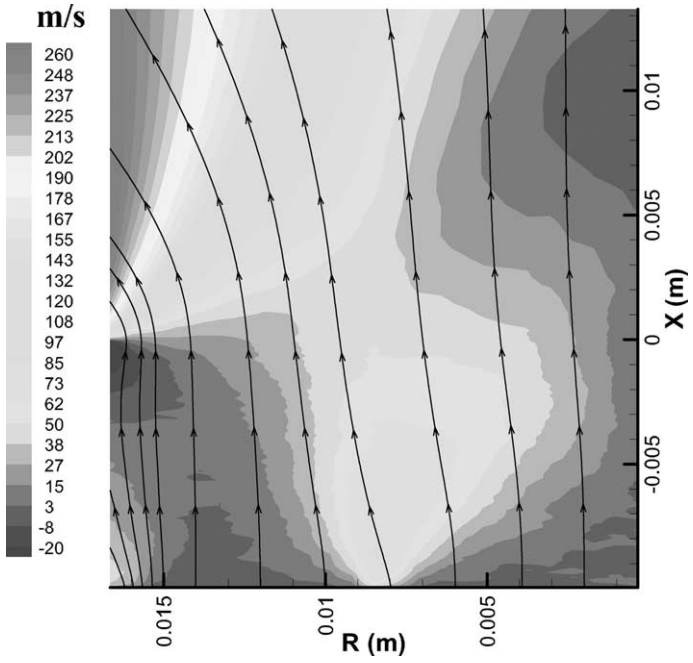

Fig. 5. Radial velocity of the uranium–iron mixture in and above the crater without kinetic–fluid coupling.

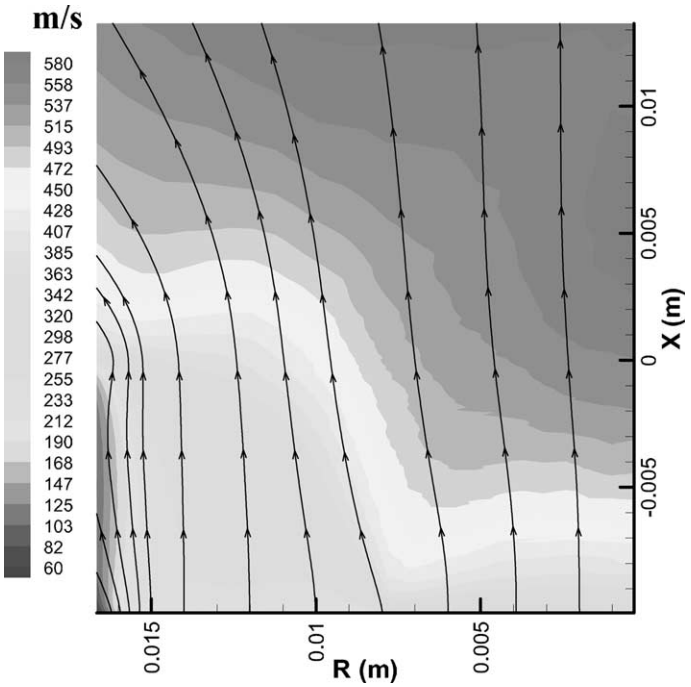

Fig. 6. Axial velocity of the uranium–iron mixture in and above the crater without kinetic–fluid coupling.

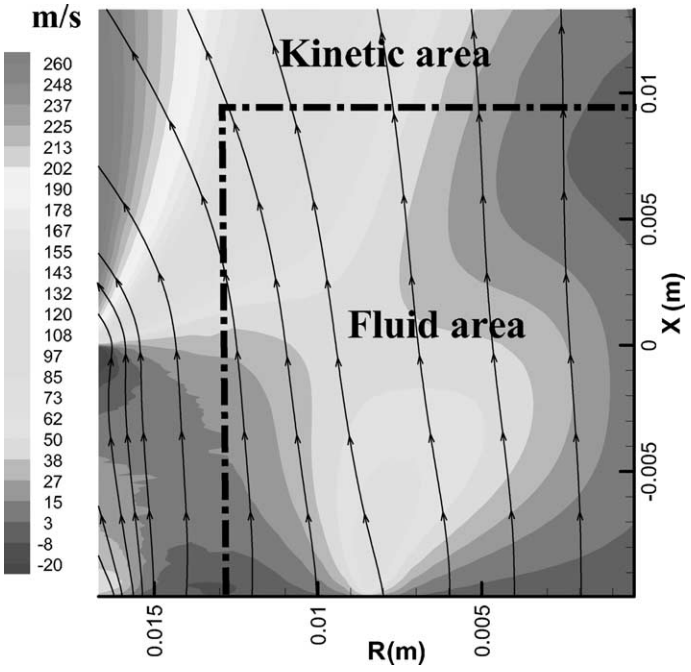

Fig. 7. Radial velocity of the uranium–iron mixture in and above the crater with kinetic–fluid coupling.

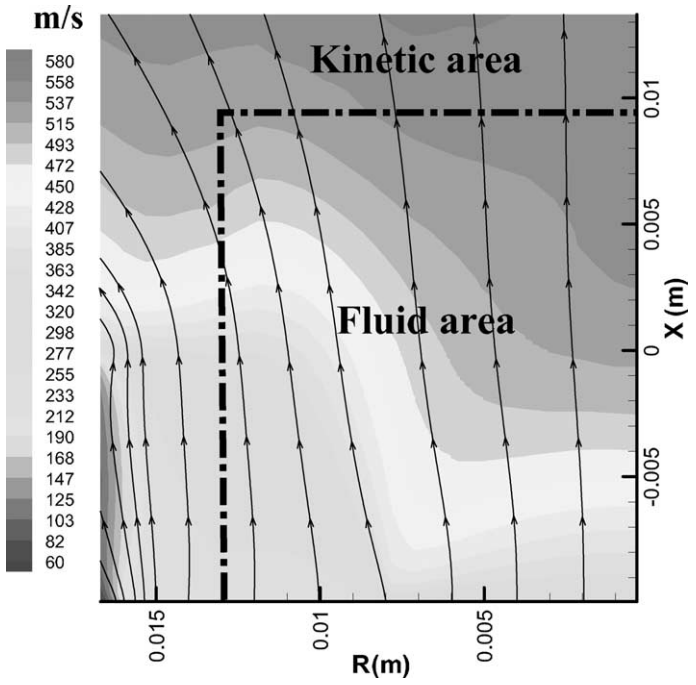

Fig. 8. Axial velocity of the uranium–iron mixture in and above the crater with kinetic–fluid coupling.

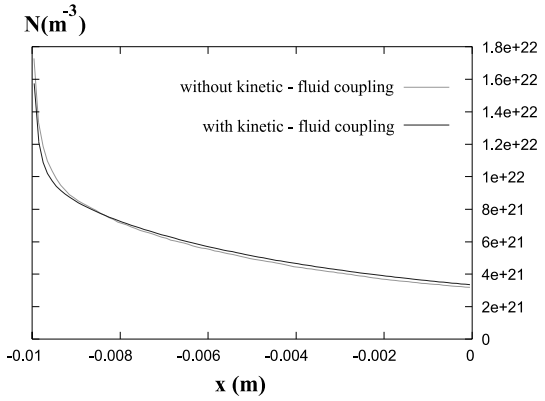

Fig. 9. Uranium density in the crater at $r = 5 \times 10^{-3}$ m with and without kinetic–fluid coupling.

Fig. 9 shows the uranium density with and without kinetic–fluid coupling at the radius $r = 5 \times 10^{-3}$ m (see Fig. 4) in the crater; Fig. 10 shows the uranium temperatures T_r and T_x without kinetic–fluid coupling and the mixture temperature T with kinetic–fluid coupling (and, thus, given by the Euler system) at the same radius in the crater.

Let us remark that Fig. 10 shows that the exit of the Knudsen layer is at about $x = -8 \times 10^{-3}$ m. It exists also a (bidimensional) Knudsen layer parallel to the X-axis near the frontier of the crater which is at the temperature of 3000 K (see Fig. 4) but we do not have tested yet the asymptotic matching of the fluid

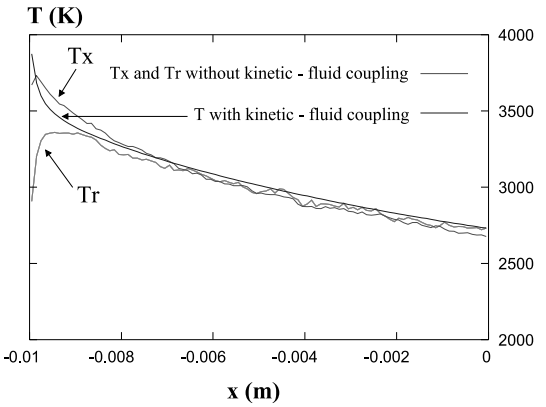

Fig. 10. Uranium temperature in the crater at $r = 5 \times 10^{-3}$ m with and without kinetic–fluid coupling.

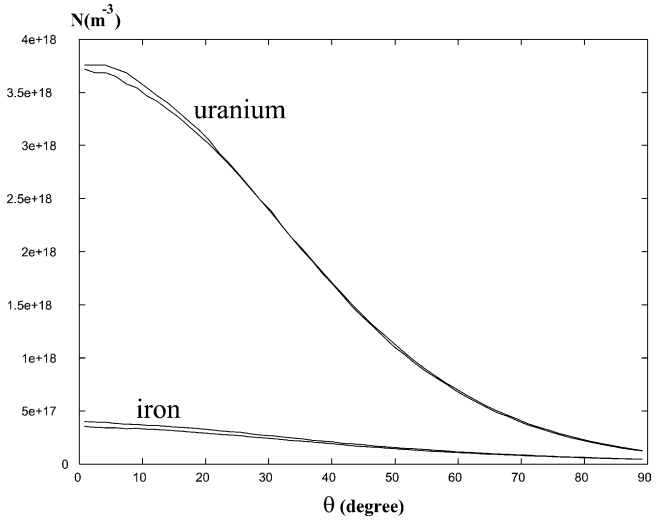

Fig. 11. Uranium and iron densities in the rarefied area (cf. also Fig. 3) with and without kinetic–fluid coupling.

domain on that frontier (see the kinetic–fluid interface on Fig. 4). Moreover, let us note that this frontier is more a condensation surface than an evaporation source because of the direction of trajectories of the gas mixture (see Fig. 5 for example).

Fig. 11 shows the uranium and iron densities at a distance of 0.5 m from the crater and, thus, in the rarefied area (see also Fig. 3).

Fig. 12 shows the population ratio of uranium atoms at the second level with and without kinetic–fluid coupling at the heights of 0.12 and of 0.35 m from the crater where laser absorption measurements are performed (see also Fig. 3). Let us note that this population ratio is the number of uranium atoms at the second level $v = 620$ cm^{-1} compared to the number of uranium atoms at the fundamental level $v = 0$.

All these results show that the kinetic–fluid coupling algorithm gives very good results since they are quasi similar to those obtained without kinetic–fluid coupling. Moreover, the Marshak conditions used to asymptotically match the fluid domain on the uranium–iron source allows to almost obtain the real

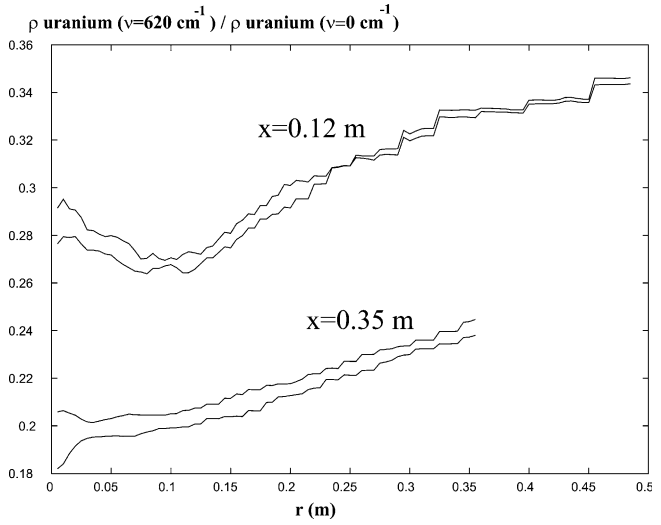

Fig. 12. Uranium population ratio where it is done laser absorption measurements (cf. Fig. 3) with and without kinetic–fluid coupling.

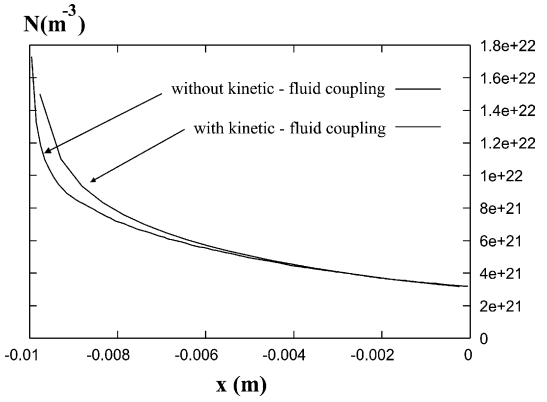

Fig. 13. Uranium density in the crater at $r = 5 \times 10^{-3}$ m with and without kinetic–fluid coupling, and with a coarse mesh in the Euler domain.

macroscopic quantities in the Knudsen layer (when the mesh in the fluid domain is not modified, see also below) *although we solve the Euler system in this layer*: this result is *notable*, all the more reason we take into account a non-Maxwellian boundary condition (62b) at the part of the uranium source $\mathscr{S}_{\mathrm{U-Fe}}$ which is impacted by the electronic beam.

5.3.2. Coarse mesh in the fluid domain with kinetic–fluid coupling

The size of a mesh in the crater domain is now much more important than the mean free path: in Fig. 4, the number of rectangular meshes is equal to 130×25; for the present numerical test, this number is of 50×25 (i.e., there are now many less meshes in the crater in the X-direction). Figs. 13 and 14 show that we do not obtain the macroscopic quantities in the Knudsen layer with the accuracy of the results presented in the previous Figs. 9 and 10. But, we almost recover all the macroscopic quantities near the exit of the

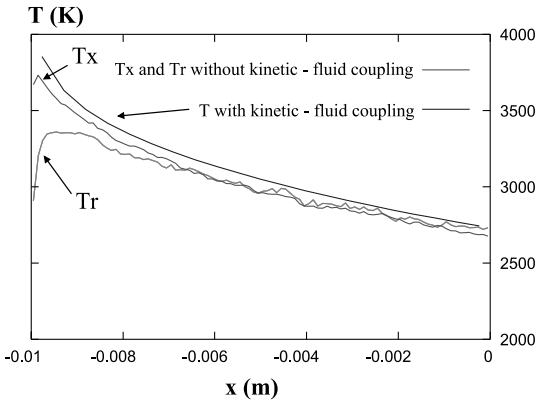

Fig. 14. Uranium temperature in the crater at $r = 5 \times 10^{-3}$ m with and without kinetic–fluid coupling, and with a coarse mesh in the Euler domain.

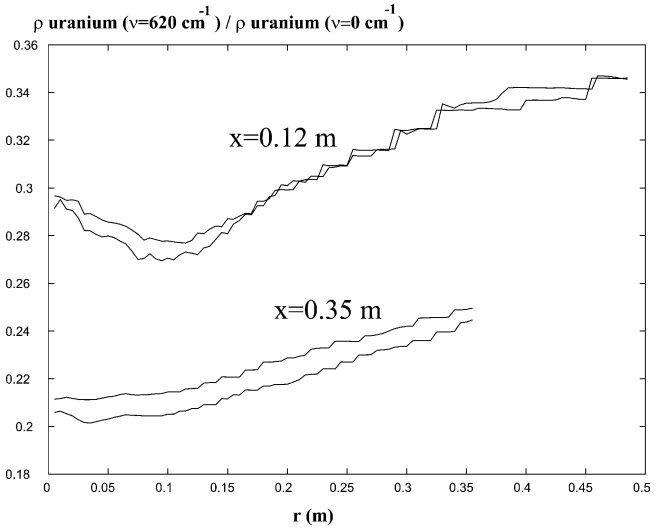

Fig. 15. Uranium population ratio where it is done laser absorption measurements (cf. Fig. 3) with and without kinetic–fluid coupling, and with a coarse mesh in the Euler domain.

Knudsen layer, i.e., at about $x = -8 \times 10^{-3}$ m. Moreover, we can see that the population ratio of uranium atoms at the second level at the heights of 0.12 and 0.35 m is still accurate: compare Fig. 15 with Fig. 12. This shows that the Marshak condition is a robust and accurate boundary condition, at least for our problem.

5.3.3. Gain in CPU time and in computer memory

By solving the Euler system in the dense area and by asymptotically matching the Euler domain on the uranium–iron source, we have divided by about 3 the CPU time. Moreover, the gain in computer memory is of about 30%: indeed, since we do not solve the Wang Chang–Uhlenbeck equations in the fluid domain, the number of particles used in the Monte-Carlo simulation is very less important.

Let us recall that the Monte-Carlo algorithm in the kinetic domain is based on the PTMC method (see [6,7] and the references herein). This Monte-Carlo algorithm is well adapted to *stationary* situations where there are *very different* mean free paths, a classical Bird algorithm having greater difficulties to converge in the high density area in AVLIS applications (although it is possible to improve the efficiency of the Bird algorithm with time subcycling as in [10]). This is due to the fact that the PTMC algorithm does not give the transcient regime but converges *only* to the stationary solution by using an ergodic hypothesis. Thus, the gain in CPU time and in computer memory would be more important if the Monte-Carlo method was a classical Bird type technique.

5.3.4. Two examples of physical informations which can be obtained for the evaporation AVLIS process from the kinetic–fluid coupling algorithm with a reasonable CPU time

Example 1: effect of the iron on the uranium metastable levels. Fig. 16 shows that the population ratio of uranium atoms at the second level is diminished when there are iron atoms in the uranium gas expansion. This phenomena is well known in the AVLIS process and is directly due to the uranium–iron collisions which increase the metastable energy transfers. Thus, the kinetic–fluid coupling algorithm allows us to study the influence of the value of the iron density $n_s^k(T_s)$ in the source, and used in (63), on the population ratio of uranium atoms at the second level by doing a lot of simulations with a reasonable CPU time and without loss of accuracy.

Example 2: effect of the modelling of the interaction of the electronic beam with the uranium source. Instead of using the relations (62a) and (62b) to modelize the interaction of the electronic beam with the uranium atoms of the source, we can use the boundary condition

$$\phi_i^k(v) = C_{k,i}^{\mathrm{ste}}(T_s, T_*) \cdot n_s^k(T_s) \cdot \exp\left[-\frac{mv^2}{2T_s(r)} \right] \cdot g_i^k \exp\left(-\frac{m\epsilon_i^k}{T_*} \right)$$
$$\text{if } i = 1, 2 \text{ or } 3 \text{ and for all } r \geqslant 0, \tag{65}$$

where the temperature T_* in (65) is again defined by (64): we suppose here that the electrons impact all the surface $\mathscr{S}_{\mathrm{U-Fe}}$ of the crater because of multiple collisions. Fig. 17 shows that the population ratio of

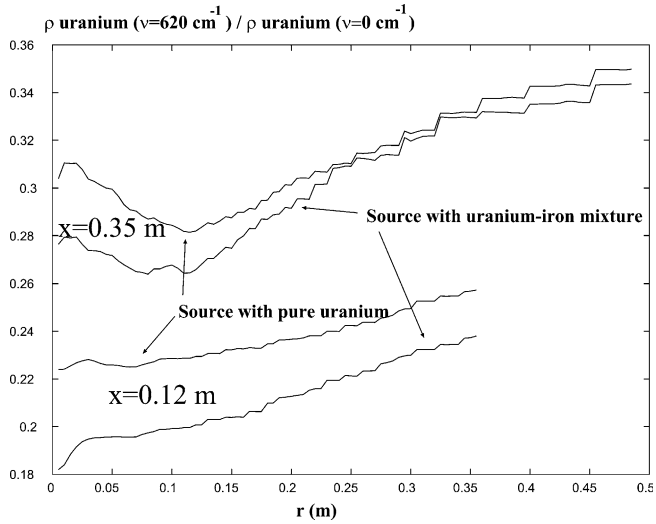

Fig. 16. Uranium population ratio where it is done laser absorption measurements (cf. Fig. 3) with kinetic–fluid coupling, and with or without iron in the uranium source.

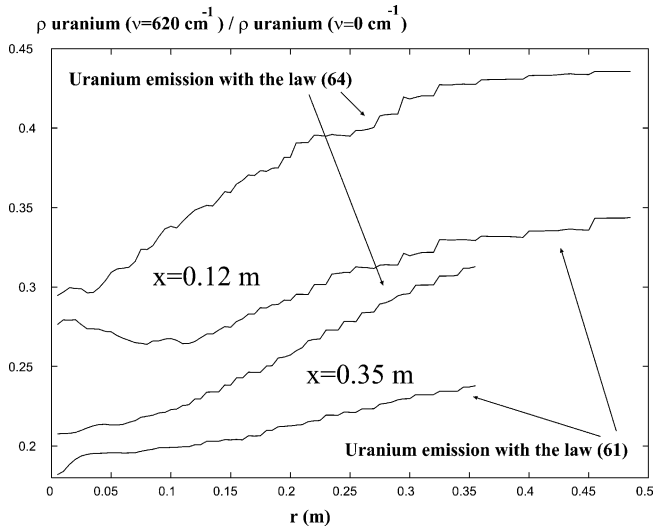

Fig. 17. Uranium population ratio where it is done laser absorption measurements (cf. Fig. 3) with kinetic–fluid coupling, and with different uranium emission laws on the uranium source.

uranium atoms at the second level at the heights $x = 0.12$ and $x = 0.35$ m is now more important. Thus, the kinetic–fluid coupling algorithm can also help to obtain a good modeling of the interaction of the electronic beam with the uranium source with a reasonable CPU time.

Remark. Application of the kinetic–fluid coupling algorithm to the study of the coma of a comet.

Because of the similarity between the gas expansion in the AVLIS process and the gas expansion in the coma of a comet (cf. [9]), phenomena which take place in the gas dynamics of a comet could be studied with numerical simulations using a similar kinetic–fluid coupling algorithm to diminish the CPU time and the required computer memory (we could do a similar remark for the simulation of a volcanic jet in a rarefied atmosphere as on the Jupiter's moon Io: cf. [10]). For example, in the AVLIS process, we find that the number of light species – i.e., the iron – compared to the number of heavy species – i.e., the uranium – is less important near the X-axis (this phenomena can be deduced from Fig. 11): the uranium expansion is more collimated than the iron expansion. This phenomena, due to a high pressure gradient in the radial direction, exists also in the coma of a comet and is called baro-diffusive effect (see [9]: in that case, the light species are H and OH, and the heavy species is H_2O). Let us note that in the macroscopic diffusive flux (48), the baro-diffusive effect is represented by the term $(1 - \frac{m_k}{m})C_k\frac{\nabla_x P}{P}$.

6. Conclusion

We have extended to the semi-classical multispecies case the kinetic–fluid coupling technique firstly proposed in [11] and we have applied this technique to the simulation of the gas expansion in the isotopic separation AVLIS process. This technique implies that the algorithm is conservative and that there is no overlapping between the kinetic and fluid domains.

From this point of view, firstly, we have proposed a kinetic scheme for the resolution of the multispecies Euler system closed with a non-classical state equation. By extending to the multispecies case the relaxation

schemes theory presented in [13], we have proposed an entropic result for this multispecies kinetic scheme, result already proposed by [16] with an other approach. Secondly, we have proposed to use a Marshak condition for the asymptotic matching of the fluid domain on the evaporation source to take into account the effect of the Knudsen layer in the resolution of the Euler system.

The numerical results show an excellent agreement between the results obtained with and without kinetic–fluid coupling and show that the Marshak condition works very well for the asymptotic matching.

At last, the CPU time was divided by about 3 and the gain in computer memory was of 30% by using the kinetic–fluid coupling algorithm for the proposed numerical tests, and without any loss of accuracy: this should help the experimenters to well understand the gas expansion in the evaporation AVLIS process by doing many numerical simulations with a moderate CPU time. Moreover, the general ideas of the kinetic–fluid coupling algorithm presented in that paper could be applied for other strong evaporation problems as those studied in [9,10].

Acknowledgements

The author wishes to thank F. Doneddu, B. Perthame and P. Roblin for the helpful discussions.

Appendix A. Kinetic fluxes for the Euler system

The kinetic fluxes of the kinetic scheme (33) are defined by

$$\begin{pmatrix} \mathfrak{I} \\ \wp \\ \aleph \end{pmatrix}_{i+1/2} = \begin{pmatrix} \mathfrak{I} \\ \wp \\ \aleph \end{pmatrix}^{+}_{i+1/2} + \begin{pmatrix} \mathfrak{I} \\ \wp \\ \aleph \end{pmatrix}^{-}_{i+1/2}.$$

And, by calculating (37) and (38) with the monodimensional Maxwellian (39), we find the following numerical half fluxes:

$$\mathfrak{I}^{+}_{i+1/2} = \frac{1}{\sqrt{2\pi}} \sqrt{\frac{P_i}{\rho_i}} \mathscr{F}(x^{+}_{i+1/2}) \rho_i,$$

$$\mathfrak{I}^{-}_{i+1/2} = -\frac{1}{\sqrt{2\pi}} \sqrt{\frac{P_{i+1}}{\rho_{i+1}}} \mathscr{F}(-x^{-}_{i+1/2}) \rho_{i+1},$$

$$\wp^{+}_{i+1/2} = \frac{P_i}{2} \mathscr{G}(x^{+}_{i+1/2}) + \frac{1}{\sqrt{2\pi}} \sqrt{\frac{P_i}{\rho_i}} \mathscr{F}(x^{+}_{i+1/2}) \rho_i u_i,$$

$$\wp^{-}_{i+1/2} = \frac{P_{i+1}}{2} \mathscr{G}(-x^{-}_{i+1/2}) - \frac{1}{\sqrt{2\pi}} \sqrt{\frac{P_{i+1}}{\rho_{i+1}}} \mathscr{F}(-x^{-}_{i+1/2}) \rho_{i+1} u_{i+1},$$

$$\aleph^{+}_{i+1/2} = \frac{P_i}{2} \cdot \frac{u_i}{2} \mathscr{G}(x^{+}_{i+1/2}) + \frac{1}{\sqrt{2\pi}} \sqrt{\frac{P_i}{\rho_i}} \mathscr{F}(x^{+}_{i+1/2}) (\rho_i E_i + P_i/2)$$

and

$$\aleph^-_{i+1/2} = \frac{P_{i+1}}{2} \cdot \frac{u_{i+1}}{2} \mathscr{G}(-x^-_{i+1/2}) - \frac{1}{\sqrt{2\pi}} \sqrt{\frac{P_{i+1}}{\rho_{i+1}}} \mathscr{F}(-x^-_{i+1/2})(\rho_{i+1} E_{i+1} + P_{i+1}/2),$$

where

$$x^+_{i+1/2} = -\frac{u_i}{\sqrt{2P_i/\rho_i}},$$

$$x^-_{i+1/2} = -\frac{u_{i+1}}{\sqrt{2P_{i+1}/\rho_{i+1}}},$$

$$\mathscr{F}(x) = \exp(-x^2) - \sqrt{\pi} x \operatorname{erfc}(x)$$

and

$$\mathscr{G}(x) = \operatorname{erfc}(x),$$

$\operatorname{erfc}(x)$ being the complementary error function defined by

$$\operatorname{erfc}(x) = \frac{2}{\sqrt{\pi}} \int_x^{+\infty} \exp(-y^2)\, \mathrm{d}y.$$

References

[1] M. Clerc, P. Plurien, in: Commission of the European Communities (Eds.), Advanced Uranium Enrichment Processes – Science, Research and Development, Report EUR 10743 EN, 1986.

[2] C.S. Wang Chang, G.E. Uhlenbeck, Transport phenomena in polyatomic gases – Report No. CM-681, University of Michigan Research Report, July 1951.

[3] L. Von Waldmann, E. Trübenbacher, Formale kinetische theorie von gasgemischen aus anregbaren molekülen, Z. Nat. 17a (1962) 363–376.

[4] R.C. Stern, N.C. Lang, Measurement of the U–Kr momentum transfer cross-section using crossed molecular beams, J. Chem. Phys. 70 (4) (1979) 1802–1810.

[5] J.B. Anderson, J.D. Foch, M.J. Shaw, R.C. Stern, B.J. Wu, Statistical theory of electronic energy relaxation, in: V. Boffi, C. Cercignani (Eds.), Rarefied Gas Dynamics, vol. 1, Teubner, Stuttgart, 1986, pp. 413–421.

[6] P. Roblin, A. Rosengard, T.T. Nguyen, Model of electronic energy relaxation in the test-particle Monte-Carlo method, in: J. Harvey, G. Lord (Eds.), Rarefied Gas Dynamics, vol. 2, Oxford University Press, Oxford, 1995, pp. 522–528.

[7] P. Roblin, C. Gonella, S. Chatain, Experimental measurements in gadolinium and copper atomic gas mixture flow during electron beam evaporation. Comparison with test-particle Monte-Carlo simulations, in: C. Shen (Ed.), Rarefied Gas Dynamics, Beijing University Press, 1997, pp. 940–945.

[8] A. Nishimura, Application of direct simulation Monte-Carlo method for analysis of AVLIS evaporation process, in: Proceedings of the 6th International Symposium on Advanced Nuclear Energy Research, Mito (Japan), edited by Japan Atomic Energy Research Institute, JAERI-CONF 95-005, 1995, pp. 375–383.

[9] A.A. Pyarnpuu, V.I. Shematovitch, S.B. Svirschevsky, E.V. Titov, Nonequilibrium jet flows in the coma of a comet, in: C. Shen (Ed.), Rarefied Gas Dynamics, Beijing University Press, 1997.

[10] J. Zhang, D.B. Goldstein, P.L. Varghese, N.E. Gimelshein, S.F. Gimelshein, D.A. Levin, Modeling low density sulfur dioxide jets: application to volcanoes on Jupiter's moon Io, AIAA 1 (2001) 2767.

[11] J.F. Bourgat, P. Le Tallec, B. Perthame, Y. Qiu, Coupling Boltzmann and Euler equations without overlapping, in: Sixth Conference IUTAM on Domain Decomposition Methods for Partial Differential Equations, AMS Providence, Como, Italy, June 1992.

[12] A. Klar, H. Neunzert, J. Struckmeir, Particle methods and domain decomposition, in: C. Shen (Ed.), Rarefied Gas Dynamics, Beijing University Press, 1997, pp. 263–272.
[13] F. Coquel, B. Perthame, Relaxation of energy and approximate Riemann solvers for general pressure laws in fluid dynamics, SIAM J. Numer. Anal. 35 (6) (1998) 2223–2249.
[14] B. Perthame, Second order Boltzmann schemes for compressible Euler equations in one and two space dimensions, SIAM J. Numer. Anal. 29 (1) (1992) 1–19.
[15] A. In, Numerical evaluation of an energy relaxation method for inviscid real fluids, SIAM J. Sci. Comput. 21 (1) (1999) 340–365.
[16] P. Villedieu, P.A. Mazet, Schémas cinétiques pour les équations d'Euler hors équilibre thermochimique, La Recherche Aérospatiale, édition Gauthier-Villars, vol. 2, 1995, pp. 85–102.
[17] S. Dellacherie, On the Wang Chang–Uhlenbeck equations, Discr. Continous Dyn. Syst. Series B 3 (2) (2003) 229–253.
[18] S. Dellacherie, Sur le caractère entropique des schémas de relaxation appliqués à une équation d'état non classique, C.R. Acad. Sci. Paris, t. 332, série 1 (2001) 765–770.
[19] S. Dellacherie, N. Rency, Relations de fermeture pour le système des équations d'Euler multi-espèces. Construction et étude des schémas de relaxation en multi-espèces et en multi-constituants, CEA report R-5999, 2001.
[20] S. Dellacherie, Relaxation schemes for the multicomponent Euler system, M2AN (2003), submitted.
[21] S. Dellacherie, Kinetic-fluid coupling in the field of the Atomic Vapor Laser Isotopic Separation: numerical results in the case of a monospecies perfect gas, in: Rarefied Gas Dynamics, Proceedings of the 23th RGD conference, Whistler, British Columbia, 2002.
[22] E. Godlewski, P.A. Raviart, Numerical approximation of hyperbolic systems of conservation laws, in: Applied Mathematic Sciences, vol. 118, Springer, Berlin, 1996.
[23] R. Abgrall, R. Saurel, A multiphase Godunov method for compressible multifluid and multiphase flows, J. Comput. Phys. 150 (1999) 425–467.
[24] F. Golse, Applications of the Boltzmann equation within the context of upper atmosphere vehicle aerodynamics, Comput. Meth. Appl. Mech. Eng. 75 (1989) 299–316.
[25] F. Golse, F. Coron, C. Sulem, A classification of well-posed kinetic layer problem, Commun. Pure Appl. Math. XLI (1988) 409–435, see also: F. Golse, Z. Ghaoui, Une classification des couches limites cinétiques par le théorème de l'indice, C.R. Acad. Sci. Paris, t. 325, Série I (1997) 343–348.
[26] Y. Sone, Kinetic theoretical studies of the half-space problem of evaporation and condensation, Transp. Theory Statist. Phys. 29 (2000) 227–260.
[27] T. Ytrehus, Theory and experiments on gas kinetics in evaporation, in: J.L. Potter, M. Summerfield (Eds.), Rarefied Gas Dynamics, AIAA, New York, 1977, pp. 1197–1212.
[28] C.J. Knight, Theoretical modeling of rapid surface vaporization with back pressure, AIAA J. 17 (5) (1979) 519–523.
[29] C.B. Alcock, V.P. Itkin, M.K. Horrigan, Vapour pressure equations for metallic elements: 298–2500 Kelvin, Can. Metall. Quaterly 23 (1984) 309–313, see also: A. Pattoret, J. Drowart, S. Smoes, Mass spectrometric determination of heat of sublimation of uranium, Trans. Faraday Soc. 65 (1969) 98.